Extragalactic Absorption, AGN Measurements and the AGN Gamma-Ray LF

F.W. Stecker

Lab for High Energy Astrophysics

NASA/GSFC

Absorption of Cosmic Gamma Rays from Blazars

Electron-Positron Pair Production Interactions with Intergalactic Low Energy Photons; Stecker, et al. 1992, Astrophys. J. 390, L49

Active Galactic Nuclei (AGN)

Active galaxies produce vast amounts of energy from a very compact central volume.

Prevailing idea: powered by accretion onto super-massive black holes (10^6 - 10^{10} solar masses). Different phenomenology primarily due to the orientation with respect to us.

HST Image of M87 (1994)

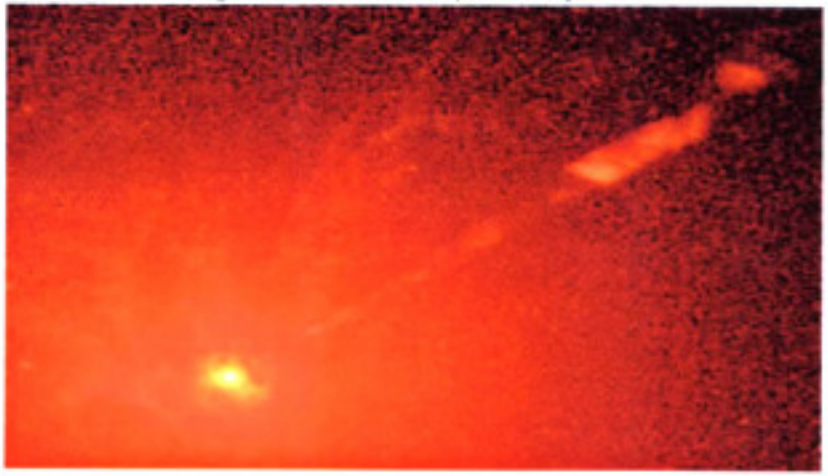

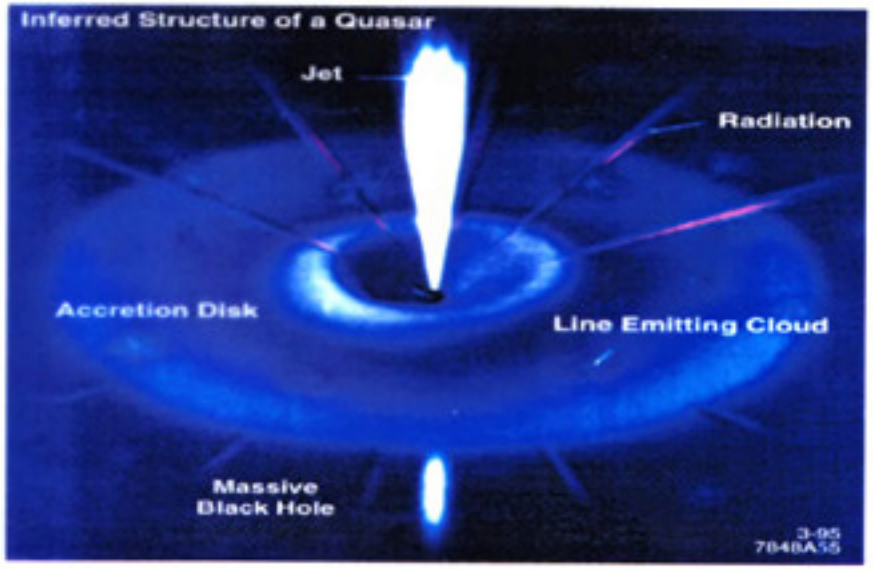

Models include energetic (multi-TeV), highly-collimated, relativistic particle jets. High energy γ-rays emitted within a few degrees of jet axis. Mechanisms are speculative; γ-rays offer a direct probe.

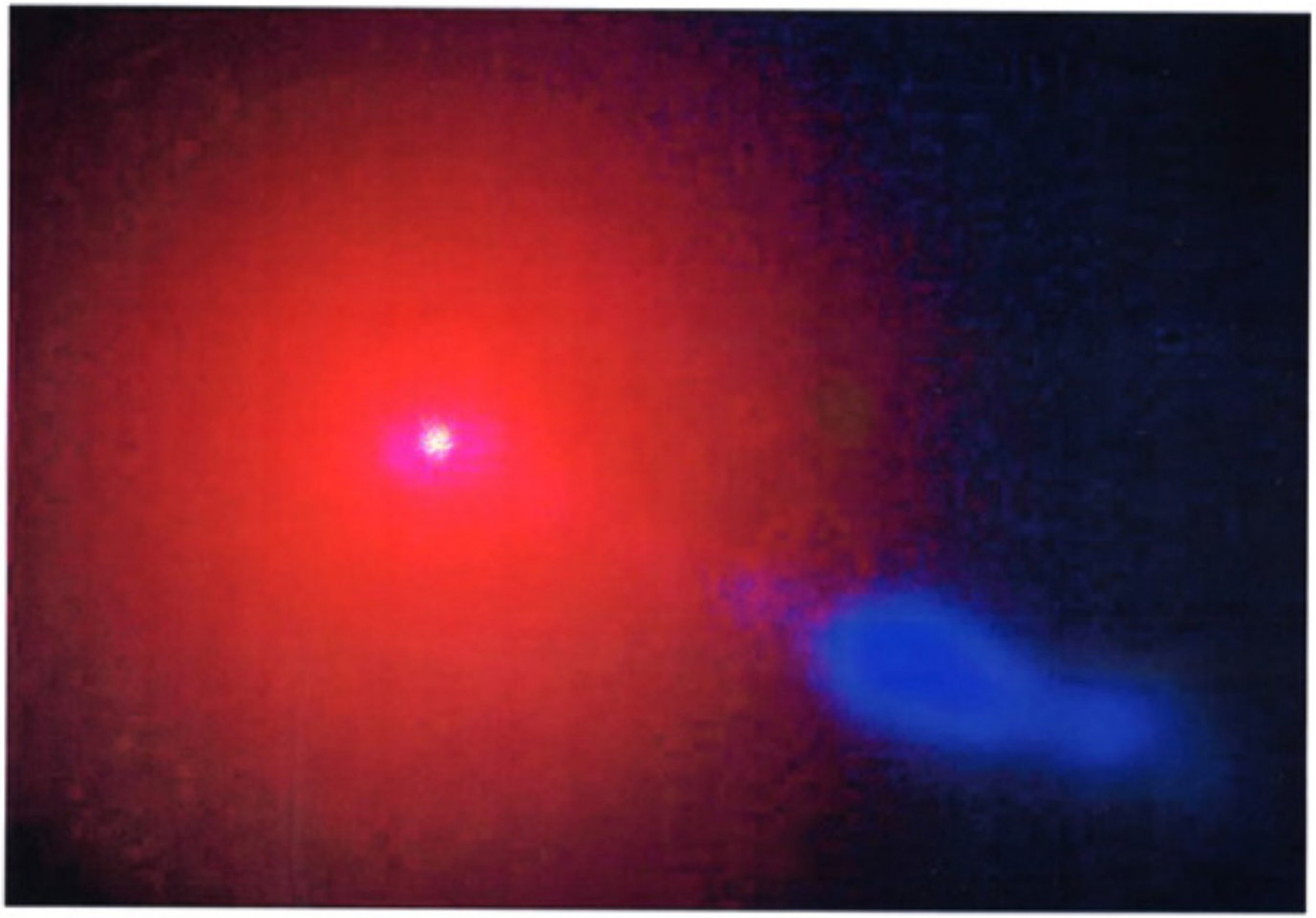

The Energetic Jet in Messier 87

VLT UT1 First Light Photo No.7

European Southern Observatory

Chandra X-Ray Observatory

PKS 1127-145

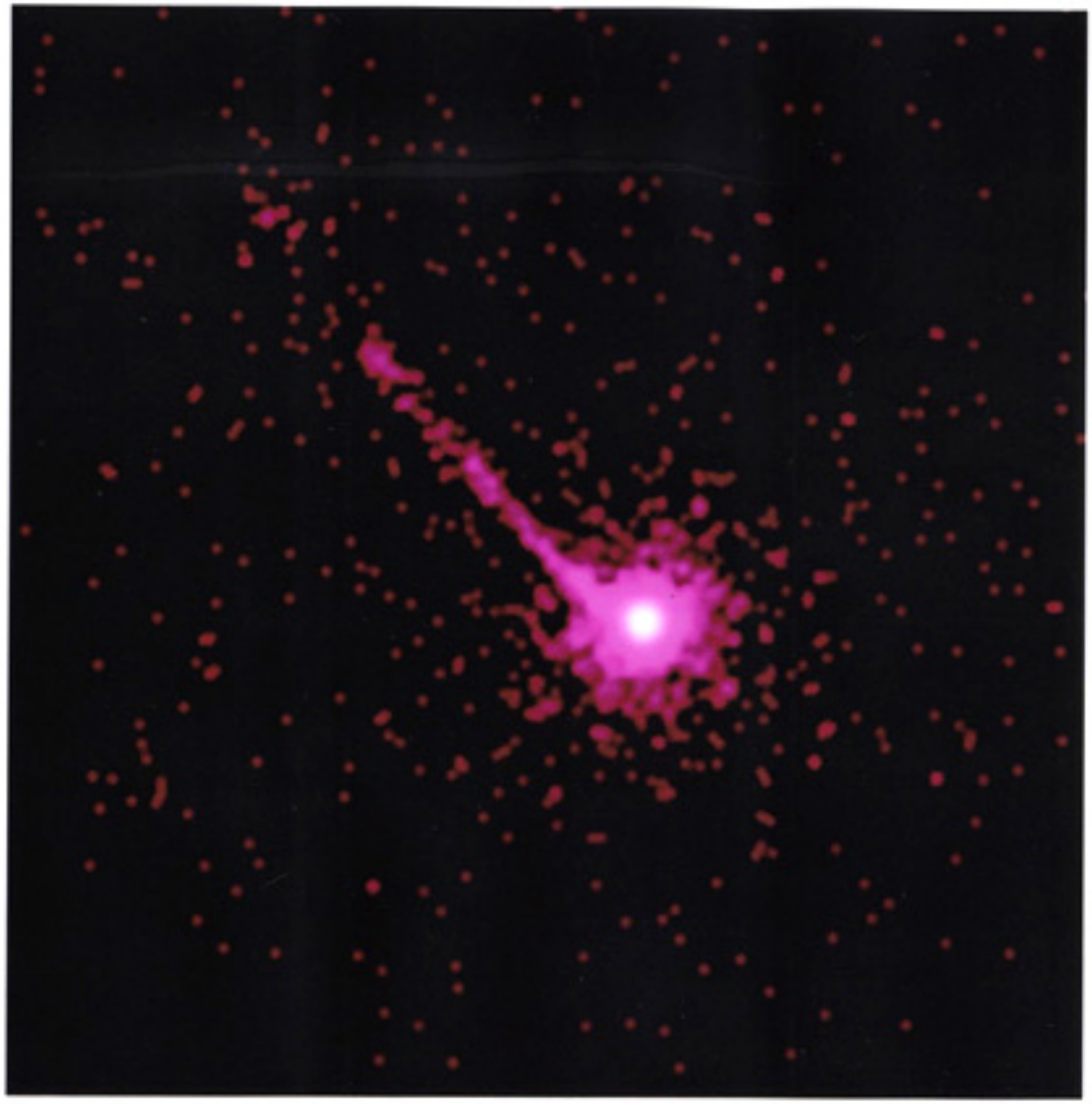

BLAZAR SCHEMATIC

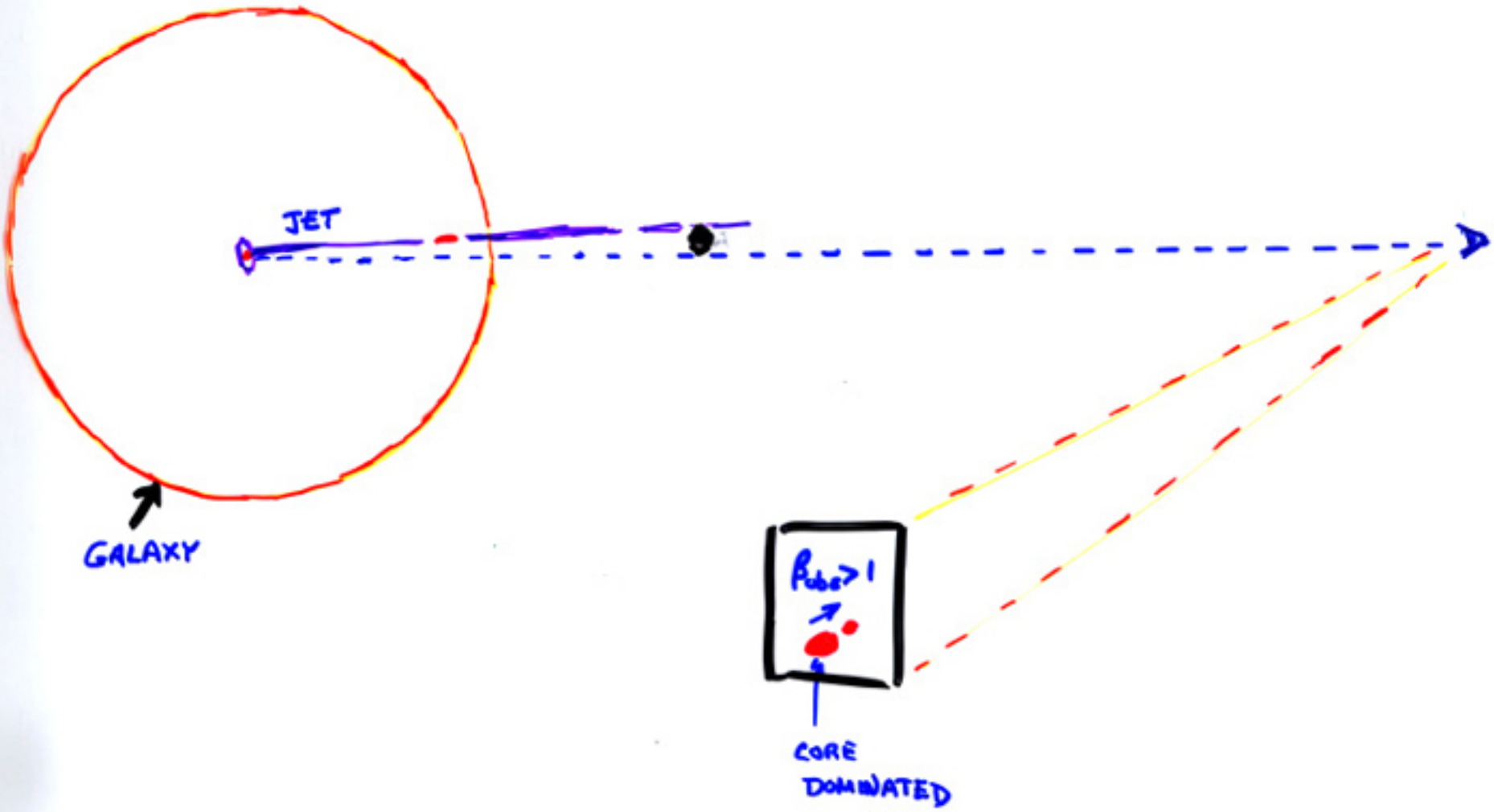

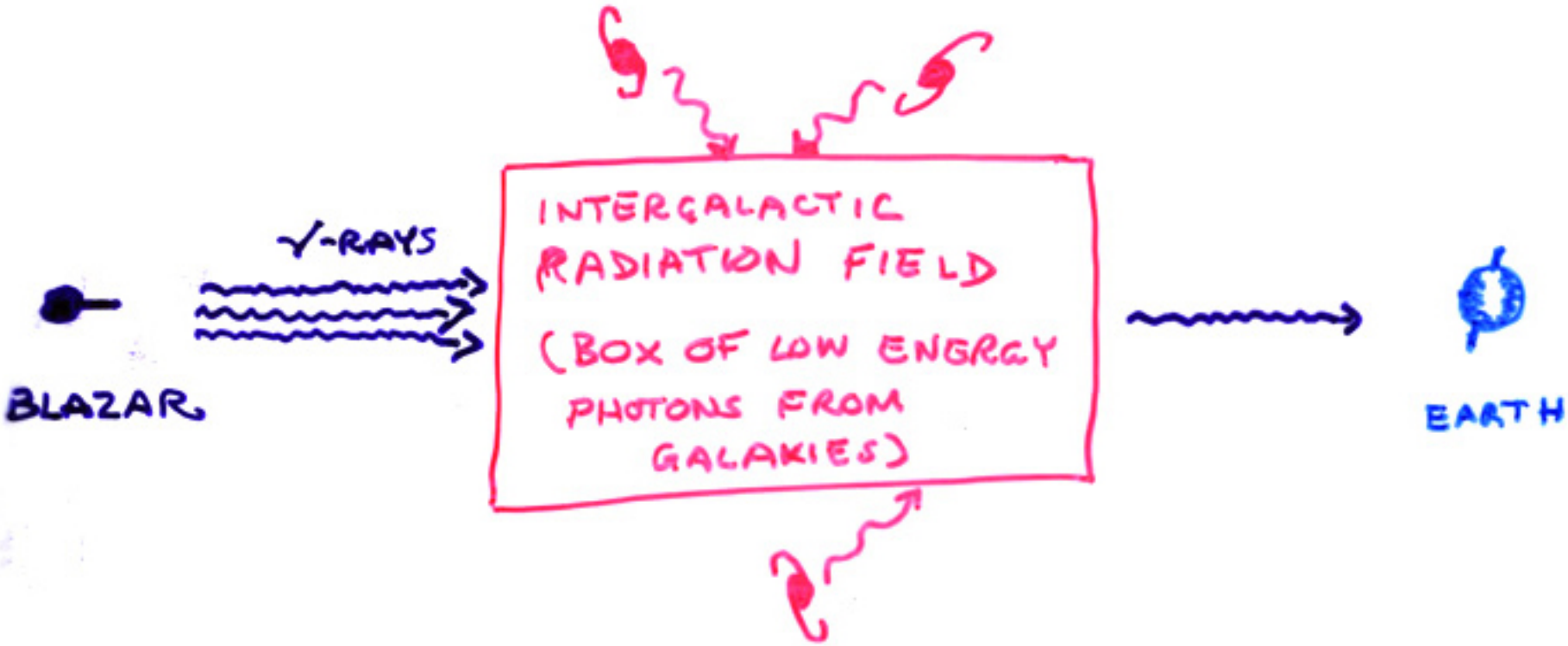

Intergalactic Absorption by γ-γ Pair-Production

γ-γ PAIR PRODUCTION

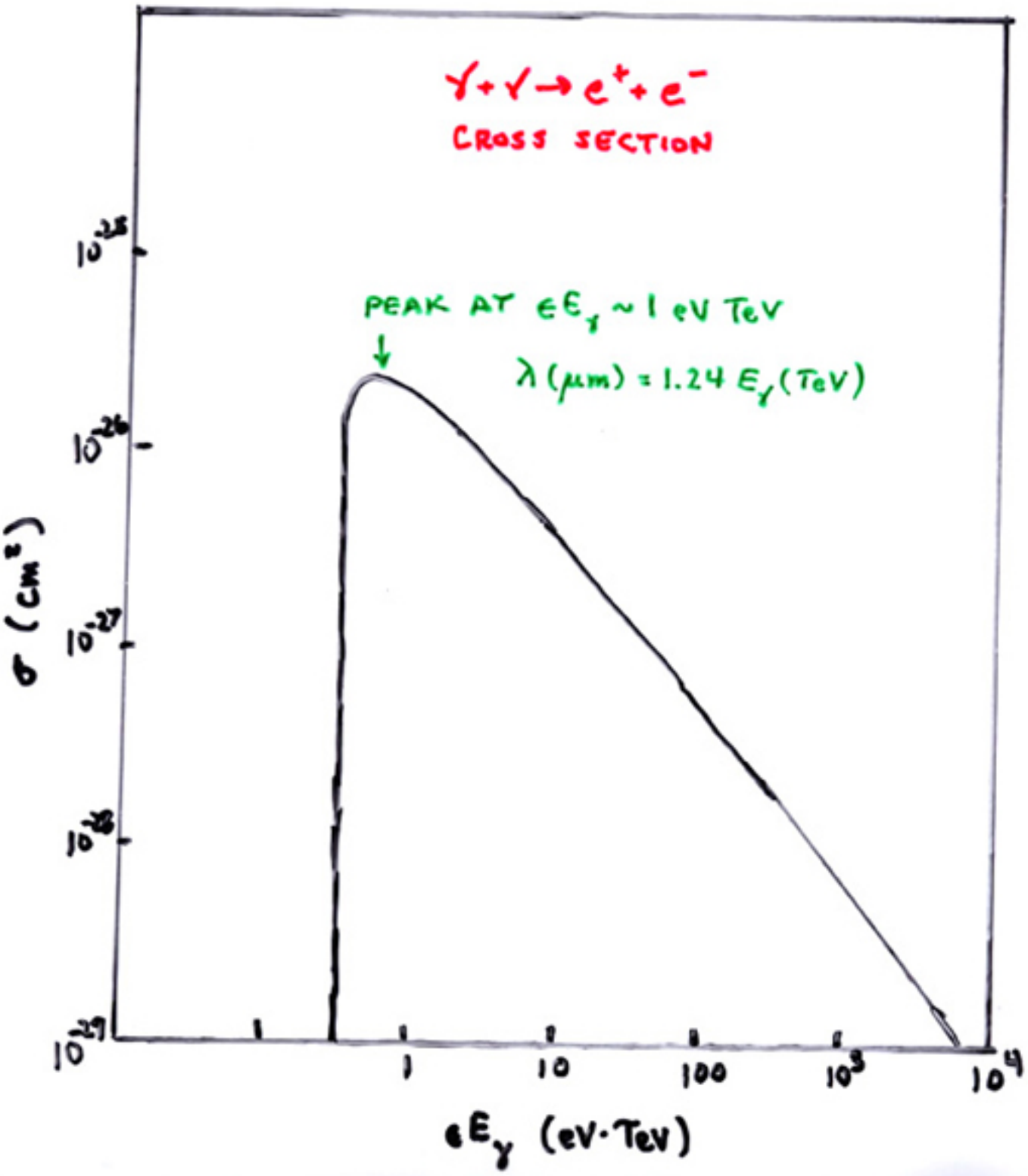

The Extragalactic IR Background

Malkan & Stecker 2001, Astrophys. J., 555, 641

Theoretical Calculations: Input

- IR Spectral Energy Distributions of Galaxies
- Galaxy Luminosity Distribution Functions (LFs) at IR Wavelengths
- Redshift Dependence of Galaxy LFs

Infrared Radiation from Galaxies

- Many galaxies contain lots of dust.
- A significant or dominant fraction of their total starlight energy is reradiated in the far-infrared after being absorbed by dust grains.
- Bright young stars are found closer to the dusty molecular clouds out of which they were born.
- This is why galaxies with higher star formation activity radiate a larger fraction of their energy in the far-infrared.

2MASS Showcase

RCW 38 A young star format
near the Vela supernova remnant

Thackeray's Globules in IC 2944

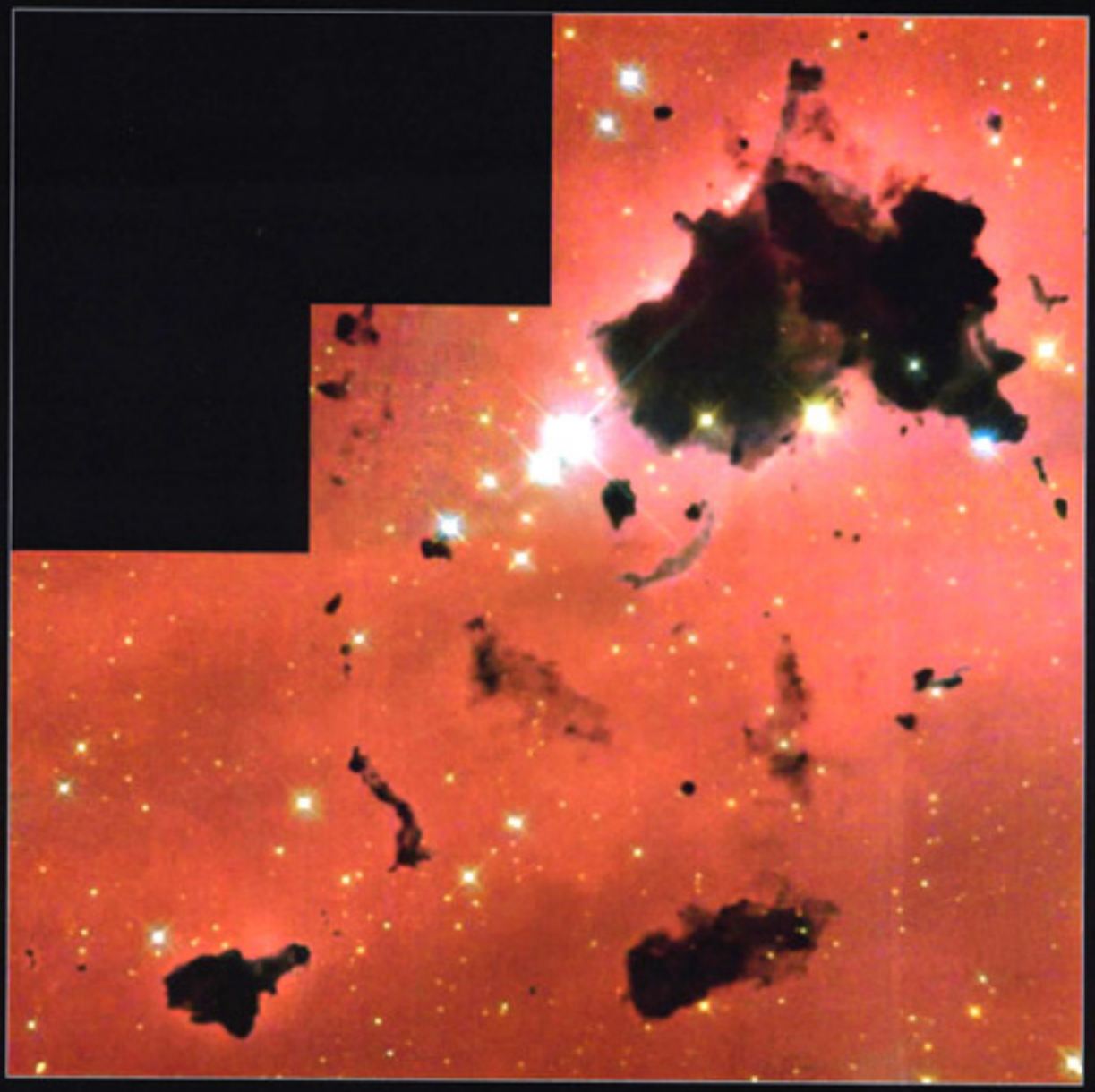

Hubble Heritage

NASA and The Hubble Heritage Team (STScI/AURA) • Hubble Space Telescope WFPC2 • STScI-PRC02-01

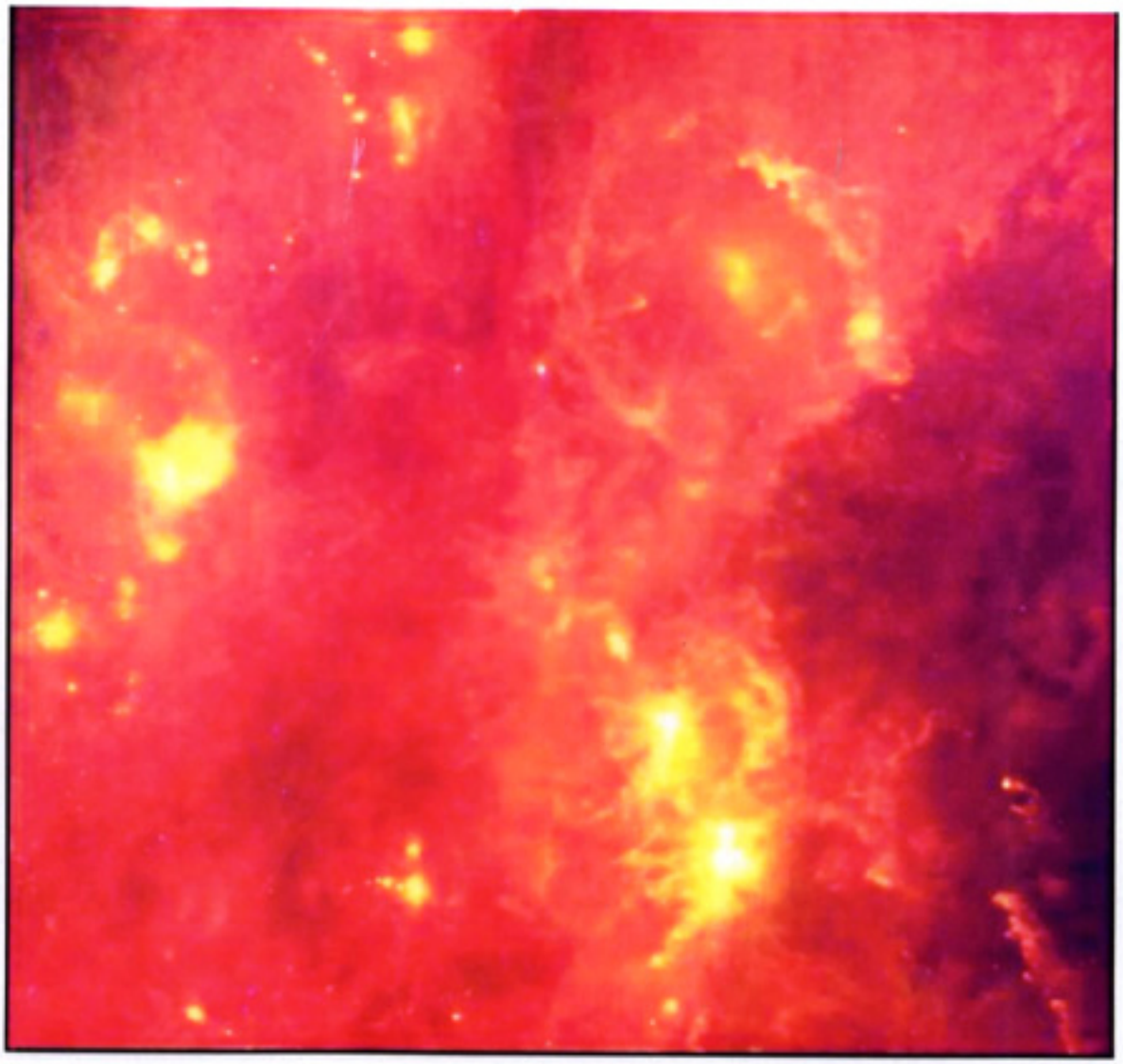

Infrared View of the star-forming Orion Region from IRAS

1) MS98 Spectral Energy Distributions

- More luminous spirals have FIR peaks which are stronger and hotter (IRAS)
- Trend continues into sub-mm: ISOPHOT

(Spinoglio etal astroph/0202331)

Uncertain at 3—10um and longward of 100um

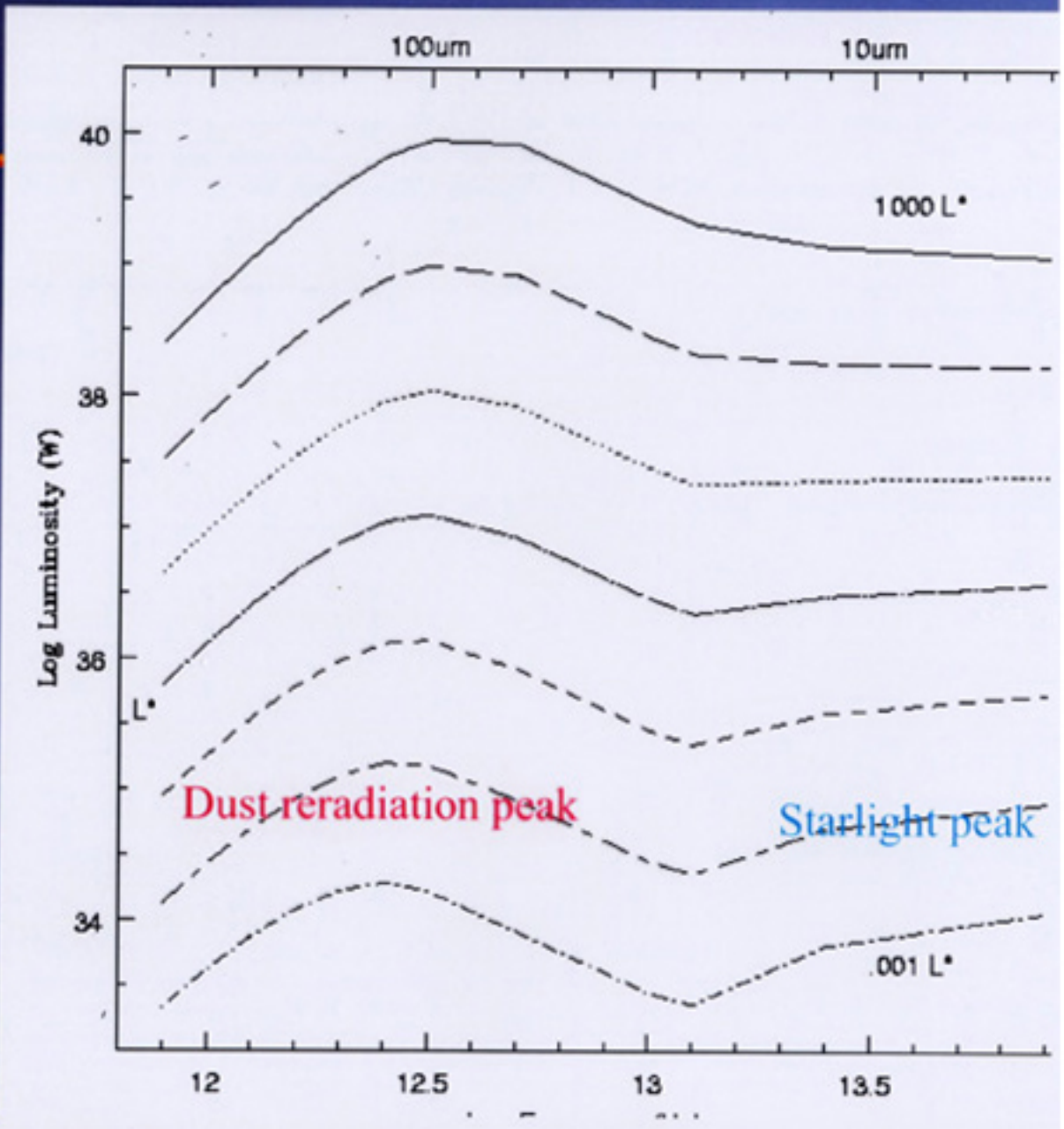

Galaxy IR Luminosity Functions

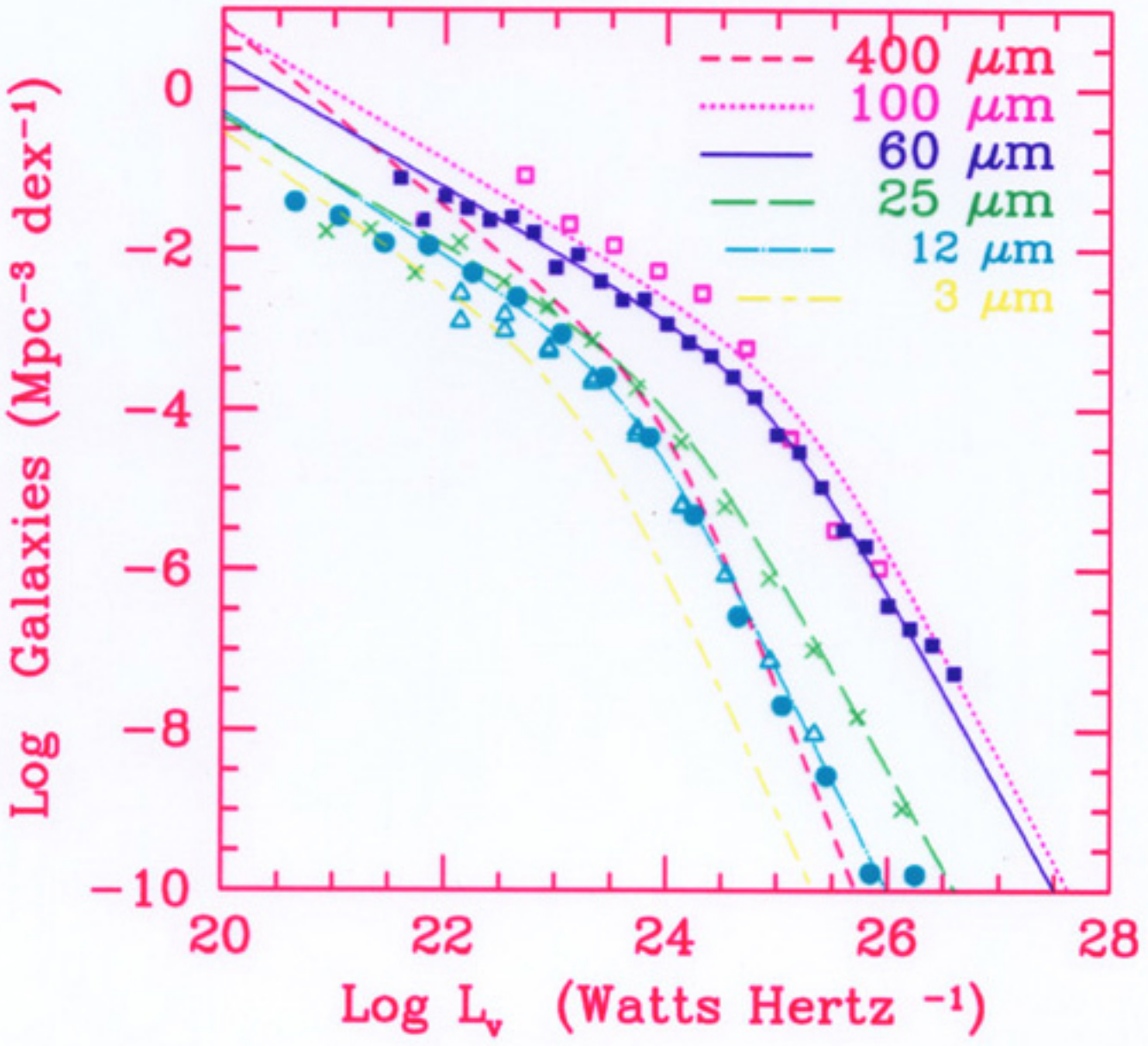

Malkan + Stecker (2001)

Redshift Dependence of Galaxy Luminosity Functions

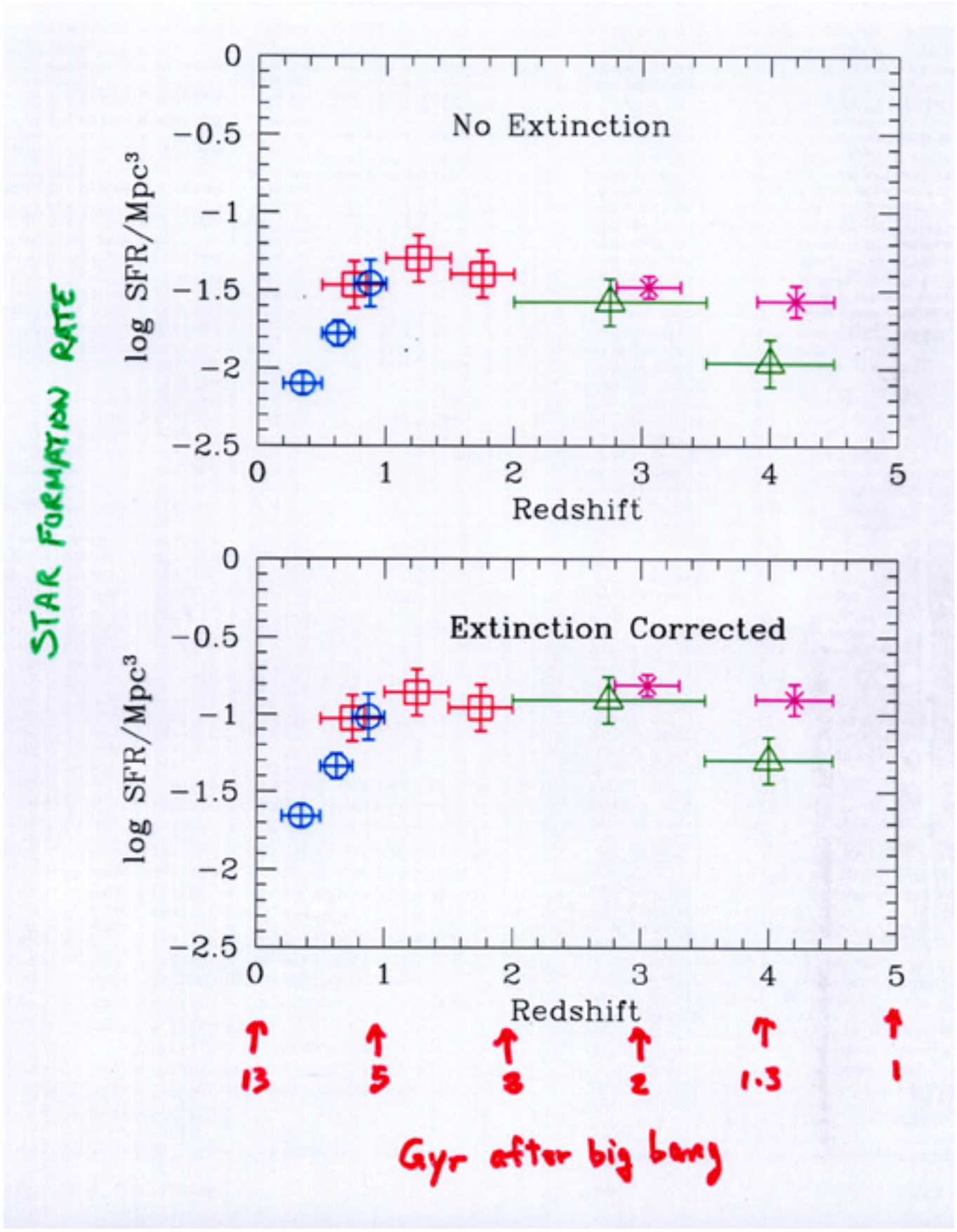
STAR FORMATION RATE
No Extinction
log SFR/Mpc³
0
−0.5
−1
−1.5
−2
−2.5
0
1
2
3
4
5
Redshift
Extinction Corrected
log SFR/Mpc³
Redshift
13
5
3
2
1.3
1
Gyr after big bang

Dust-corrected Global SFR History

Long- obs find higher SFR->not sensitive to dust

Eg: MRR 1999, with extinction corrections included

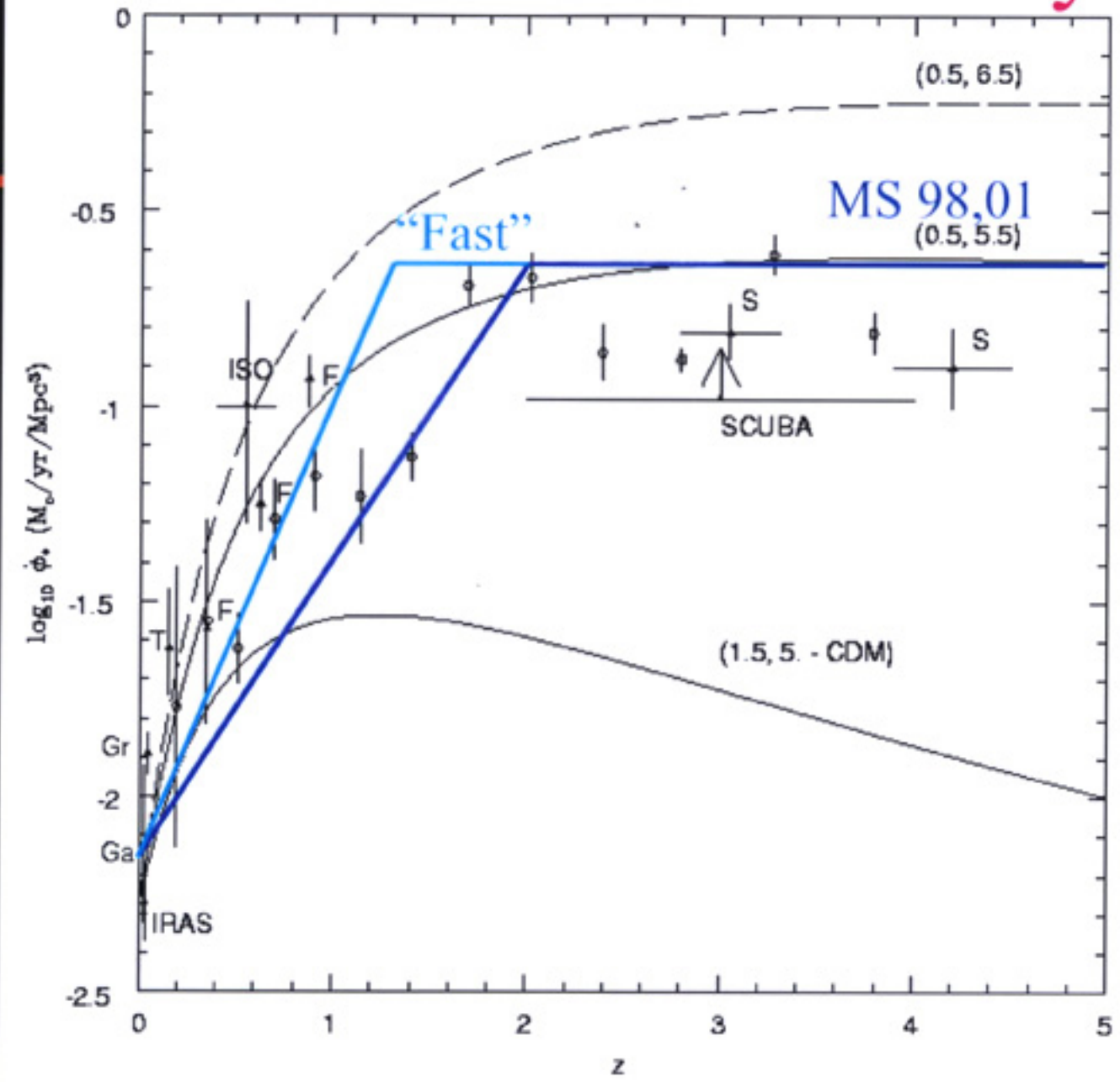

Extragalactic IR Background Observations

- Direct Measurements from COBE
- Lower Limits from Galaxy Counts
- Upper limits from TeV Gamma-Ray Observations

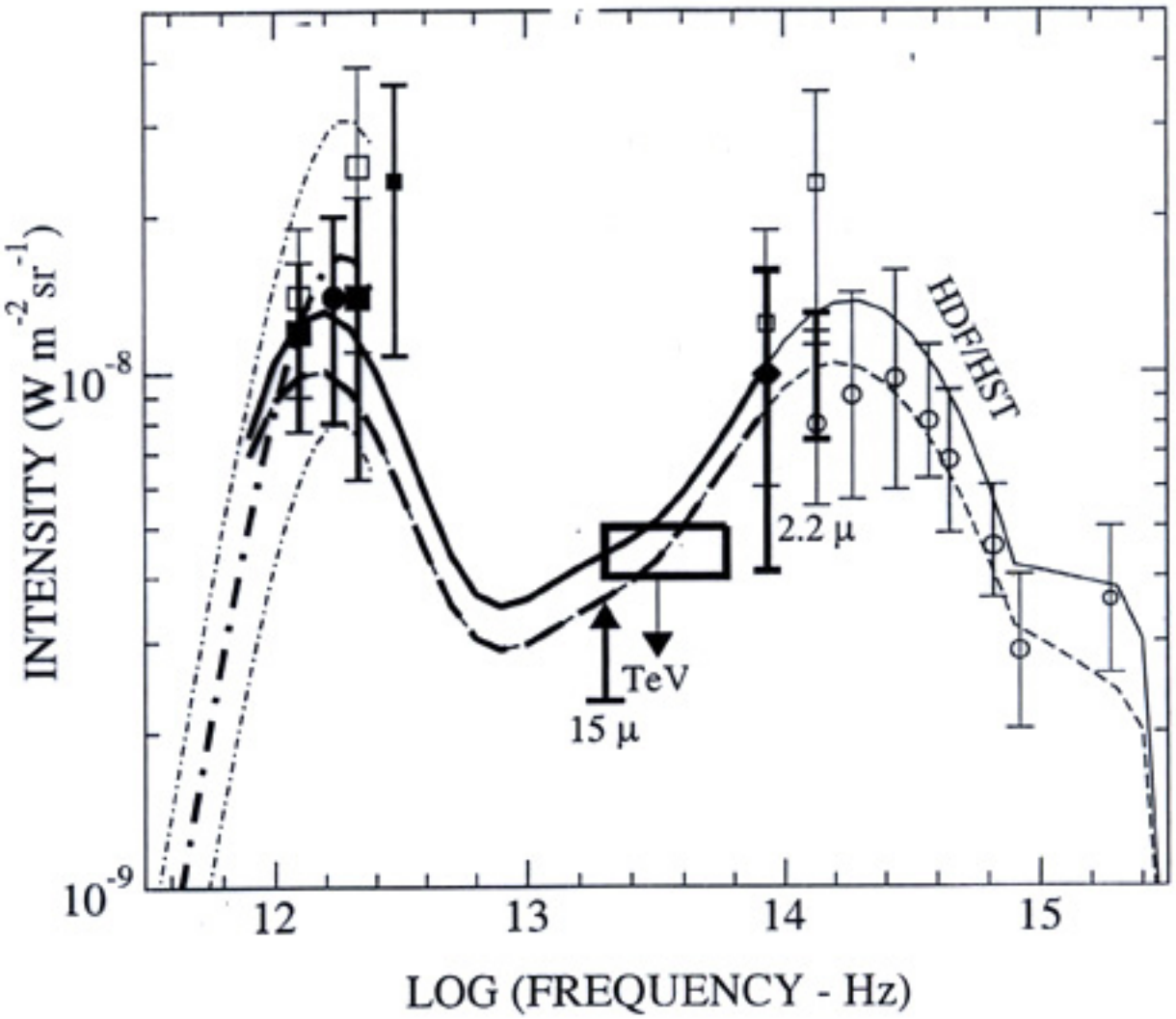
INTENSITY (W m^{-2} sr^{-1})
10^{-8}
10^{-9}
12
13
14
15
LOG (FREQUENCY - Hz)
HDF/HST
2.2 μ
TeV
15 μ

Calculated Absorption from the Present-Day Extragalactic Infrared-Optical-UV Background Radiation

De Jager & Stecker 2002

Astrophys. J. 566, 738

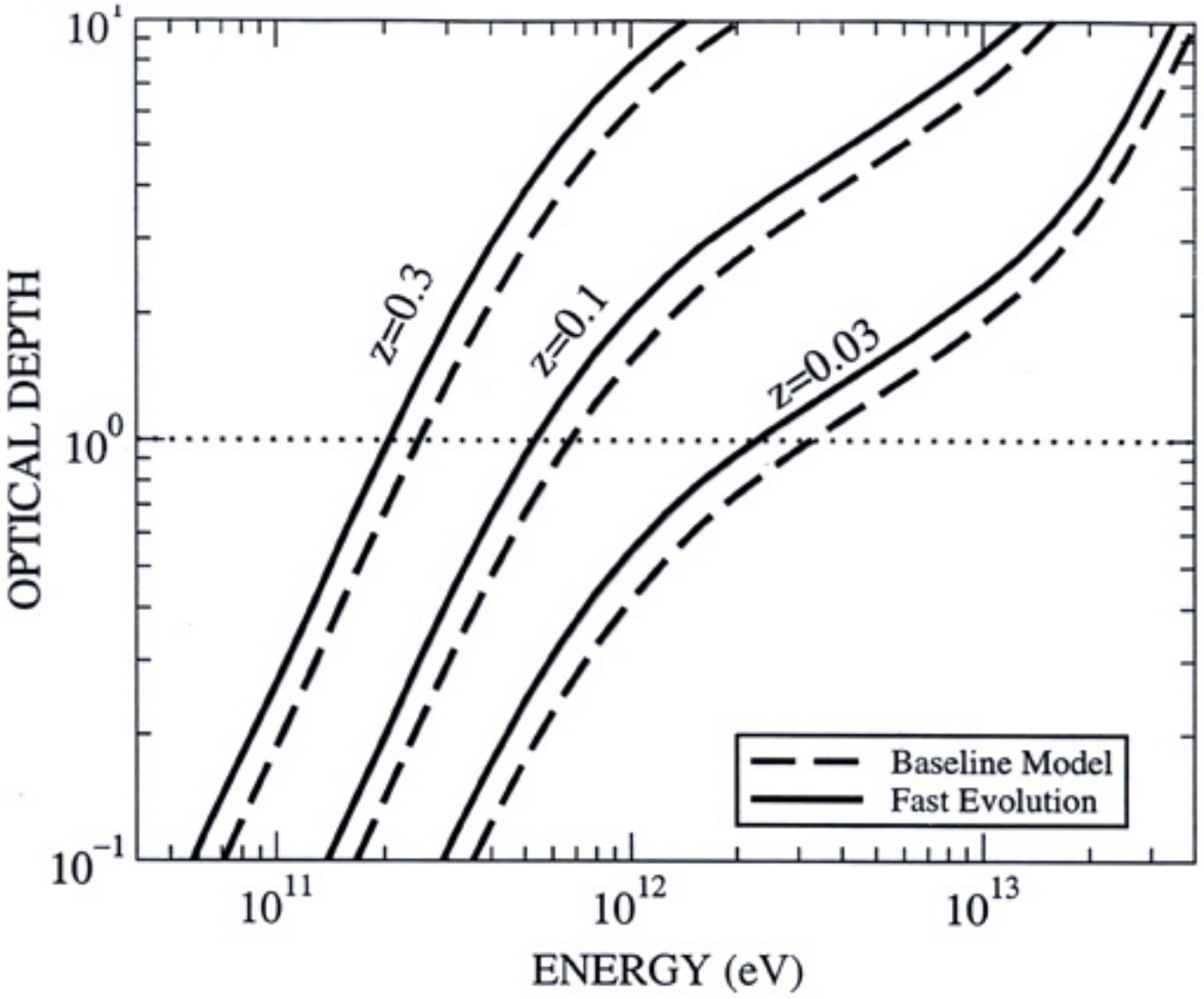
OPTICAL DEPTH
ENERGY (eV)
10^{1}
10^{0}
10^{-1}
10^{11}
10^{12}
10^{13}
z=0.3
z=0.1
z=0.03
Baseline Model
Fast Evolution

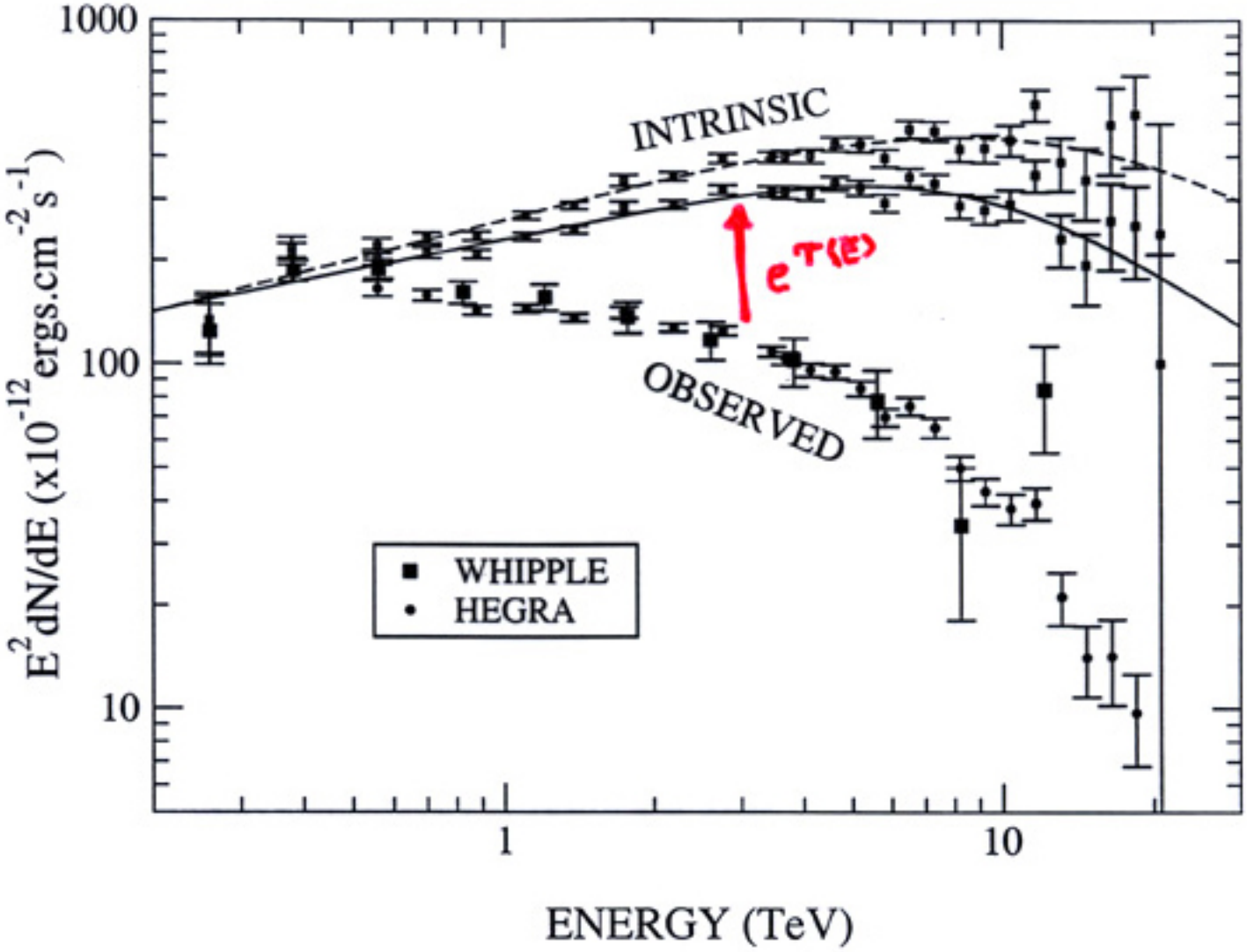
1000
100
10
1
10
INTRINSIC
OBSERVED
$e^{\tau(E)}$
WHIPPLE
HEGRA
$E^2 dN/dE$ ($x10^{-12}$ ergs.cm^{-2} s^{-1})
ENERGY (TeV)

TABLE 1. Properties of VHE blazars.

BL Lac Name	Redshift z	EGRET flux[a] (E >100 MeV) (10^{-7}cm^{-2}s^{-1})	F_X^b 2 keV (μJy)	Visible Magnitude M_V (mag)	F_R 5 GHz (mJy)
Mrk421	0.031	1.4±0.2	3.917	14.4	722
Mrk501	0.033	3.2±1.3	3.702	14.4	1371
1ES2344+514	0.044	<0.7	1.142	15.5	215
1ES1959+650	0.048		3.645	13.7	252
PKS2155-304	0.116	3.2±0.8	5.746	13.5	310
1H1426+428	0.130		2.678	16.4	38

Source: [b]Radio, optical and X-ray data from Perlman [26], [a][6, 27]

High Energy Gamma-Ray Absorption Studies: Present Results

- Have helped to fill in the gap in defining the present-day extragalactic mid-IR background spectrum from warm dust and possible hydrocarbon emission (Stanev & Franceschini 1998; Biller et al. 1998; Stecker 2002).
- Have determined the true multi-TeV energy spectra of nearby blazars (Mkn 501, Mkn 421) to allow an accurate determination of the physical parameters in their jets (de Jager & Stecker 2002; Konopelko, et al. 2002).
- Explained why only nearby ($z<0.13$) blazars are seen at TeV energies (Stecker et al. 1992).
- Have determined that special relativity holds to one part in 10^{15} at 20 TeV (Stecker & Glashow 2001) and thereby constrained quantum gravity models (Stecker 2002).

High Redshift Absorption

Salamon & Stecker 1998, ApJ 493, 547

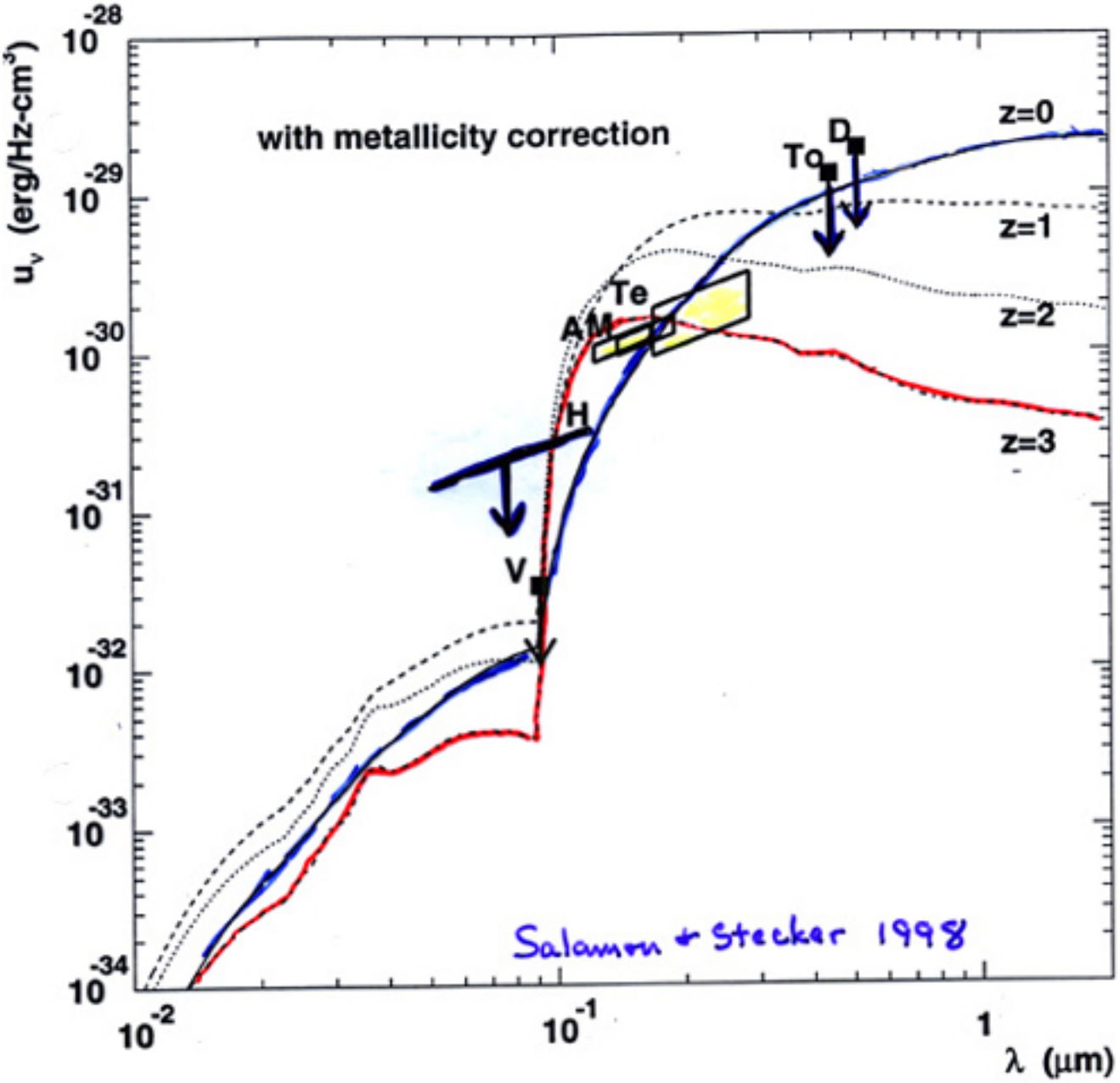

The intergalactic co-moving radiation energy density from stars, calculated with the metallicity correction factor $\mathcal{L}$ included, as a function of wavelength for redshifts $z = 0$ (solid line), $z = 1$ (dashed line), $z = 2$ (dotted line), and $z = 3$ (dot-dashed line), for a Hubble constant value of $h_0 = 0.5$. (The energy density scales as h_0)

QSO contributions to the UV energy density have a negligible effect on extragalactic gamma ray absorption, and so are neglected in our calculations. Also shown in the figure are the high-latitude measurements of Anderson *et al.* 1979 ("A"), Tennyson *et al.* 1988 ("Te"), and Martin, Hurwitz and Bowyer 1991 ("M"), and upper limits from Vogel, Weyman, and Rauch 1995 ("V"), Toller 1983 ("To"), Dube, Wickes, and Wilkinson 1979 ("D"), and Holberg 1986 ("H").

With the co-moving energy density $u_\nu(z)$ evaluated, the optical depth for γ-rays owing to electron-positron pair production interactions with photons of the stellar radiation background can be determined from the expression (Stecker, *et al.* 1992)

$$\tau(E_0, z_e) = c \int_0^{z_e} dz \frac{dt}{dz} \int_0^2 dx \frac{x}{2} \int_0^\infty d\nu (1+z)^3 \left[\frac{u_\nu(z)}{h\nu}\right] \sigma_{\gamma\gamma}[s = 2E_0 h\nu x (1+z)^2],$$

where E_0 is the observed γ-ray energy, z_e is the redshift of the γ-ray source, $x = (1 - \cos\theta)$.

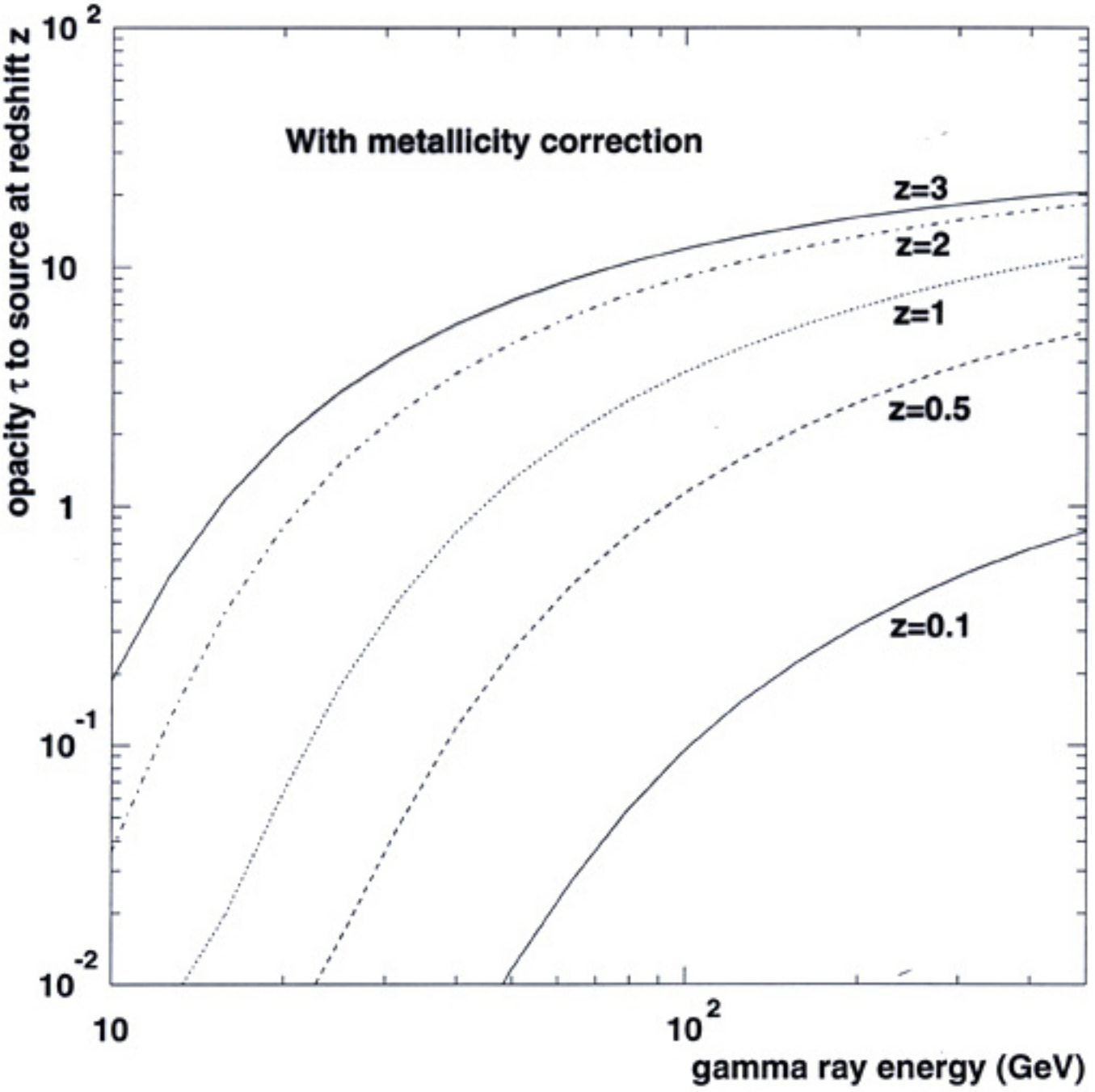

Salamon and Stecker
1998

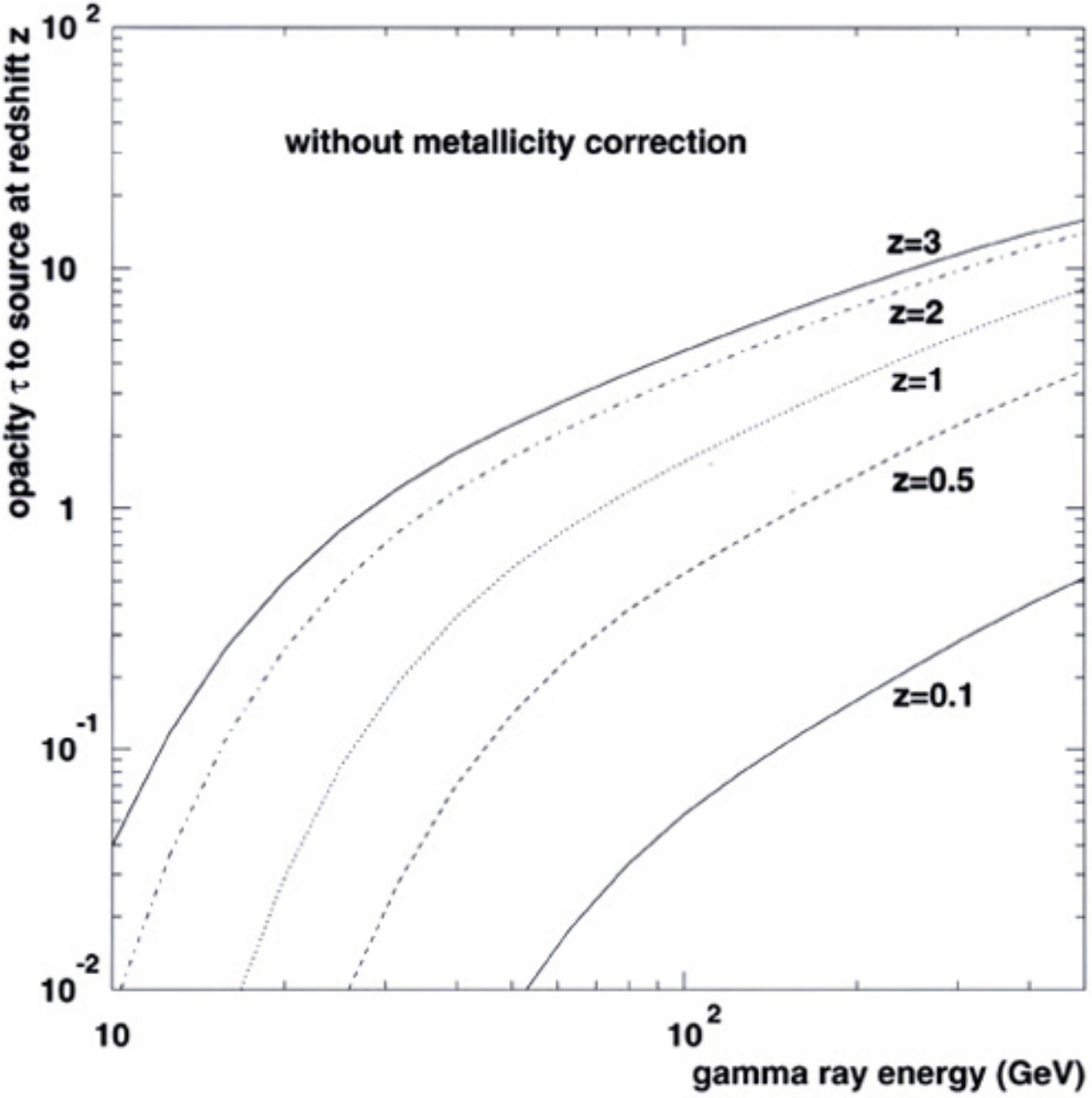
without metallicity correction
opacity τ to source at redshift z
gamma ray energy (GeV)
z=3
z=2
z=1
z=0.5
z=0.1
10 2
10
1
10 -1
10 -2
10
10 2

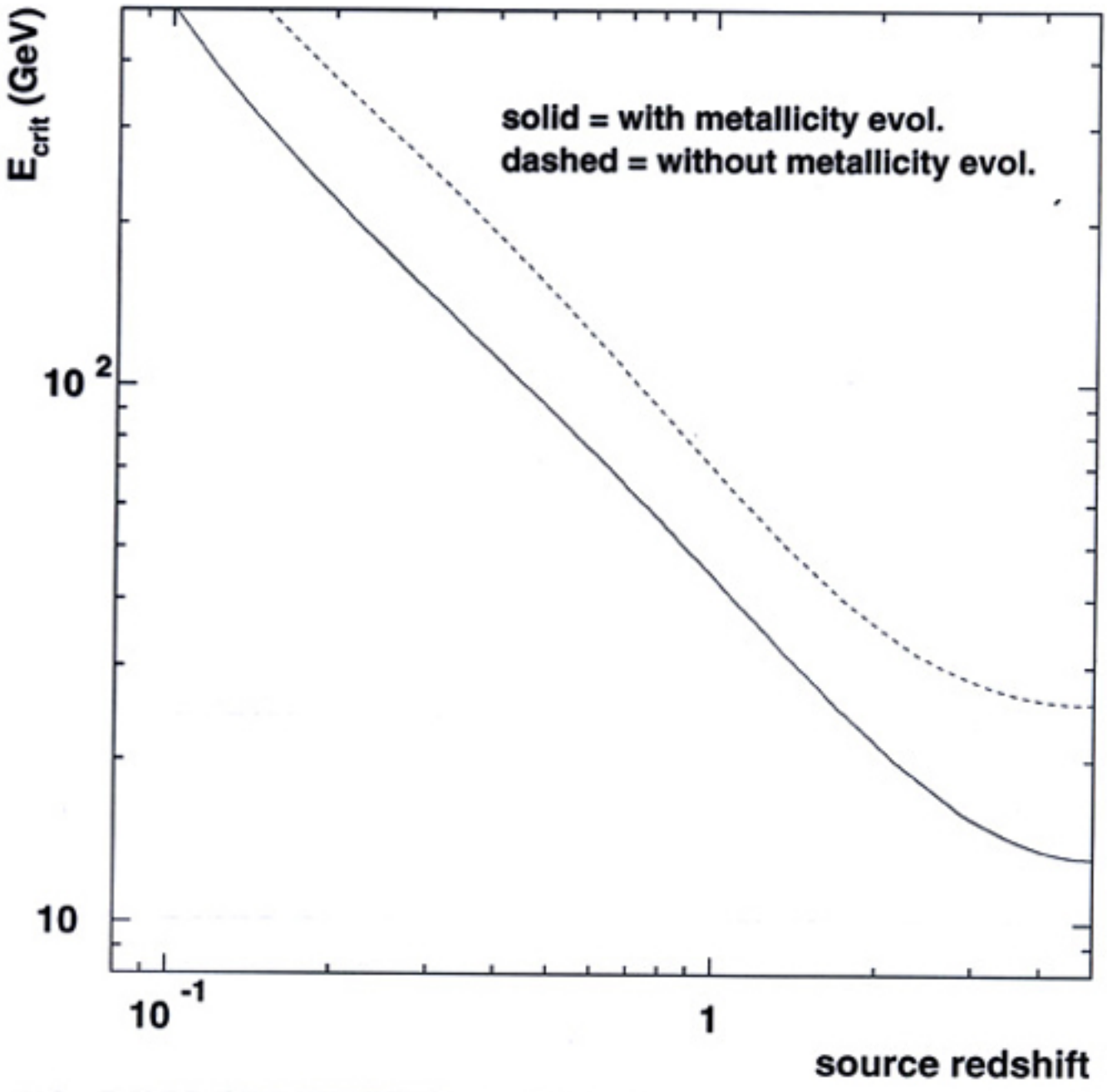

Based on results from Salamon & Stecker (1998)

Blazar Gamma-Rays and the Extragalactic Gamma-Ray Background

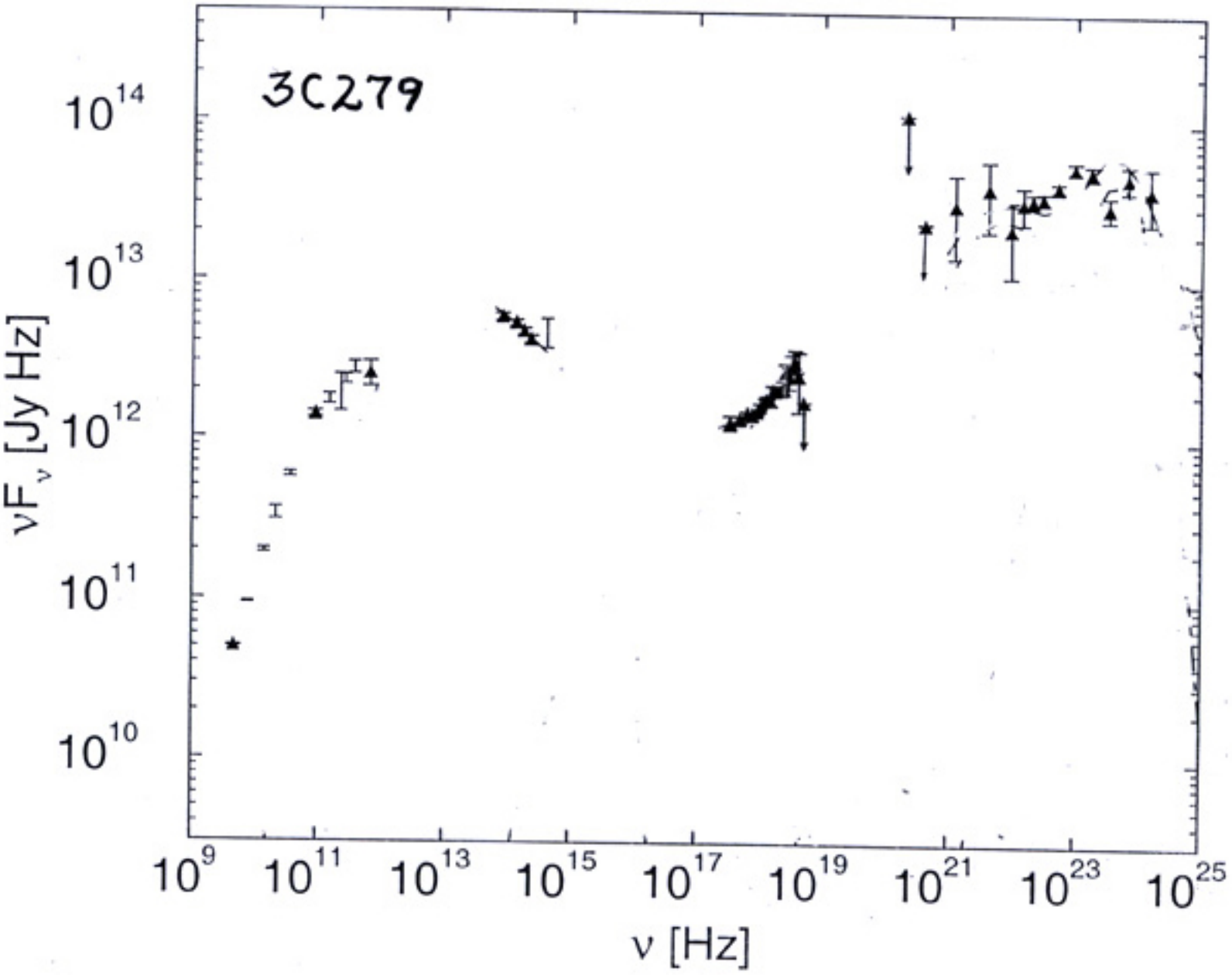
3C279
10^{14}
10^{13}
10^{12}
10^{11}
10^{10}
νF_ν [Jy Hz]
10^{9}
10^{11}
10^{13}
10^{15}
10^{17}
10^{19}
10^{21}
10^{23}
10^{25}
ν [Hz]

from Böttcher + Mukherjee 2002

Intrinsic Cutoff @ ~100GeV ??

∫ March 1998

EGRET avg.

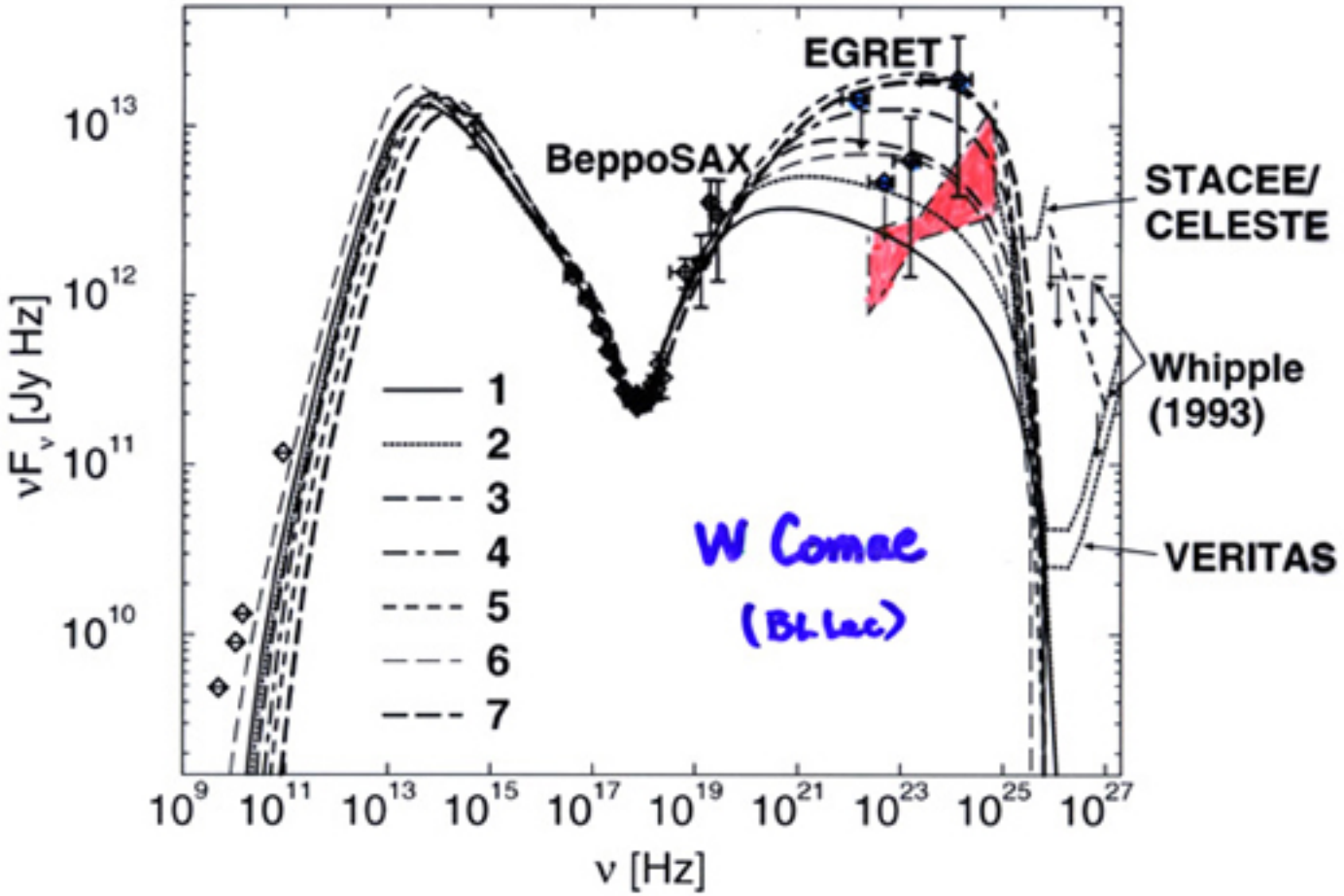

THE GAMMA-RAY BACKGROUND FROM BLAZARS: A NEW LOOK

F. W. STECKER
Laboratory for High Energy Astrophysics, NASA Goddard Space Flight Center, Greenbelt, MD 20771
AND
M. H. SALAMON
High Energy Astrophysics Institute, Physics Department, University of Utah, Salt Lake City, UT 84112

ApJ 464 (1996) 600

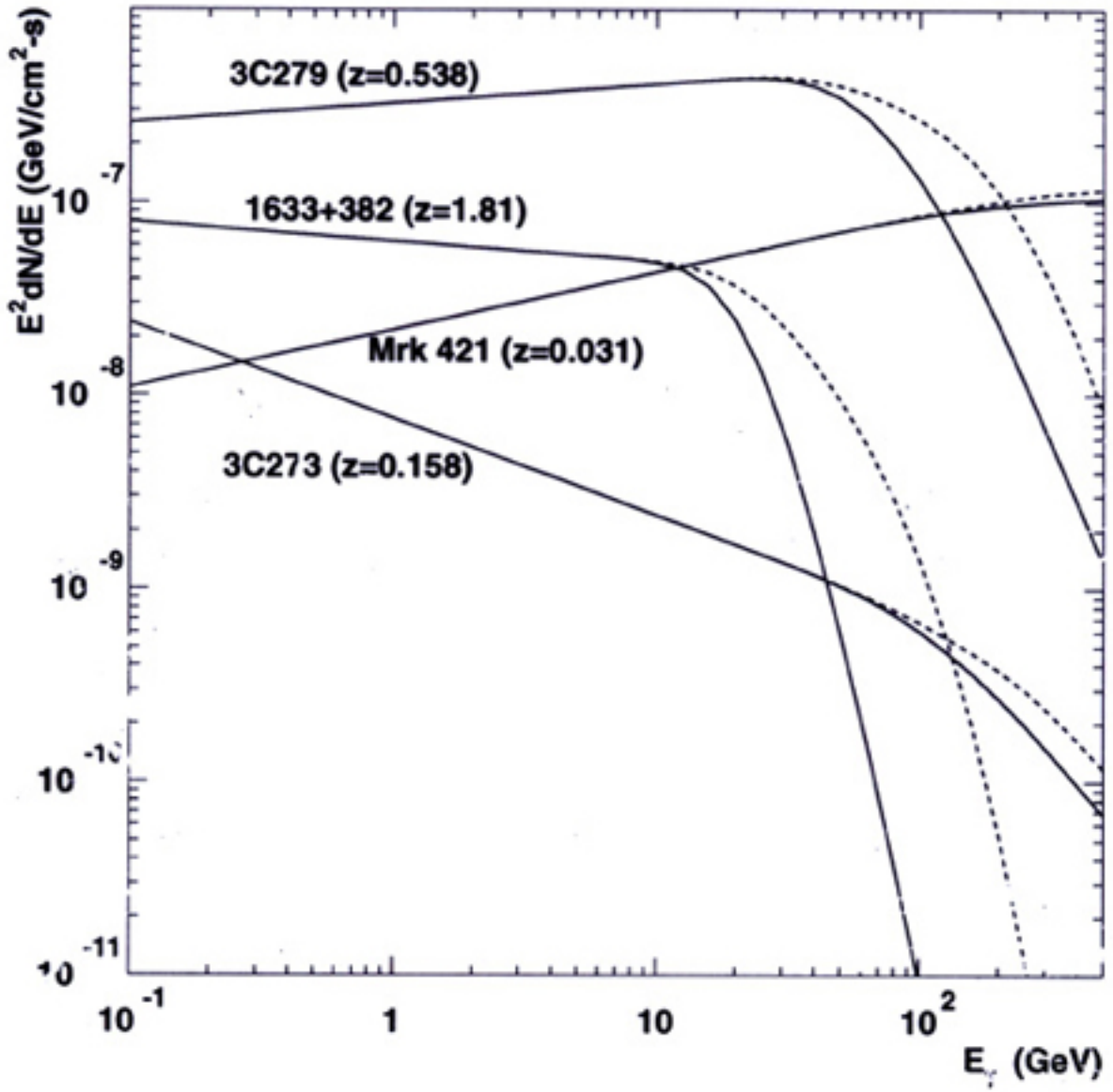

Salamon and Stecker
1998

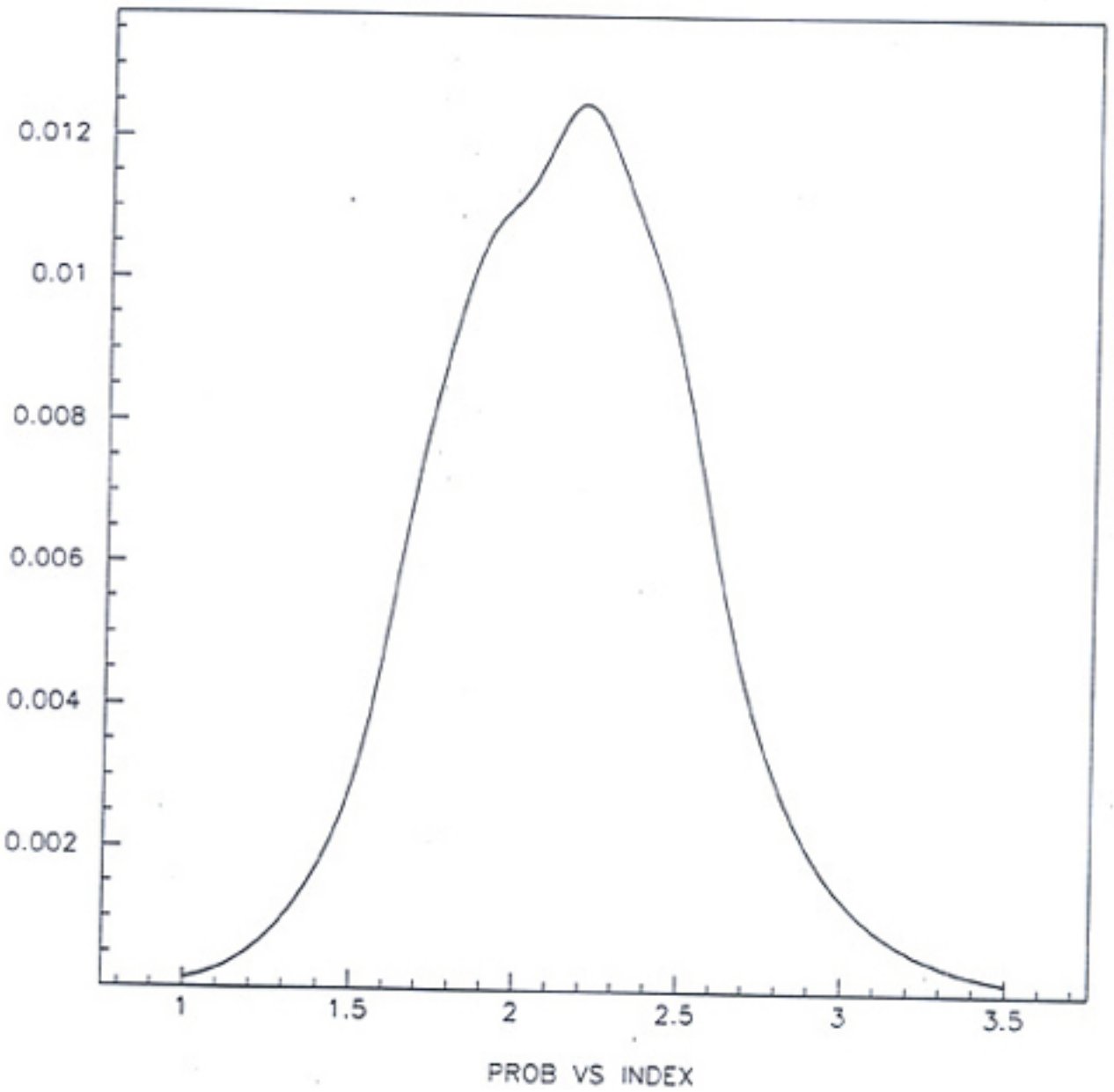

The spectral index α is defined by $E(dF/dE)(E) \propto E^{-\alpha}$, where $(dF/dE)(E)$ is the differential number flux of γ-rays at energy E; equivalently, the γ-ray differential luminosity at the source varies with γ-ray energy as $P_\gamma(E) = P_{\gamma,f}(E/E_f)^{-\alpha}$, consistent with all observed blazar γ-ray spectra. The blazars' distribution of spectral indices α is determined from the second EGRET catalog:

$$p(\alpha) = \frac{1}{N}\sum_{i=1}^{N} \frac{1}{\sigma_i\sqrt{2\pi}}\, e^{-(\alpha-\alpha_i)^2/2\sigma_i^2} ,$$

where α_i and σ_i are the catalog's spectral index and error for the ith of N blazars. We simply shift this distribution to obtain the separate distributions for the flare and quiescent states: $p^f(\alpha) = p(\alpha - \Delta\alpha_f)$, and $p^q(\alpha) = p(\alpha - \Delta\alpha_q)$, where we take $\Delta\alpha_q = 0.20$ and $\Delta\alpha_f = -0.05$, as discussed below. As there is no evidence for a change in the blazar spectral index distribution with redshift z in the EGRET catalog, we assume none.

For our analysis we use the FSRQ luminosity function of Dunlop & Peacock (1990),

$$\rho_r(P_{rf}, z) = 10^{-8.15}\left\{\left[\frac{P_{rf}}{P_c(z)}\right]^{0.83} + \left[\frac{P_{rf}}{P_c(z)}\right]^{1.96}\right\}^{-1},$$

where $\log_{10} P_c(z) = 25.26 + 1.18z - 0.28z^2$, and the units of luminosity P_r (P_γ) and comoving density ρ_r (ρ_γ) are, respectively, W Hz^{-1} sr^{-1} and Mpc^{-3} (unit interval of $\log_{10} P)^{-1}$.

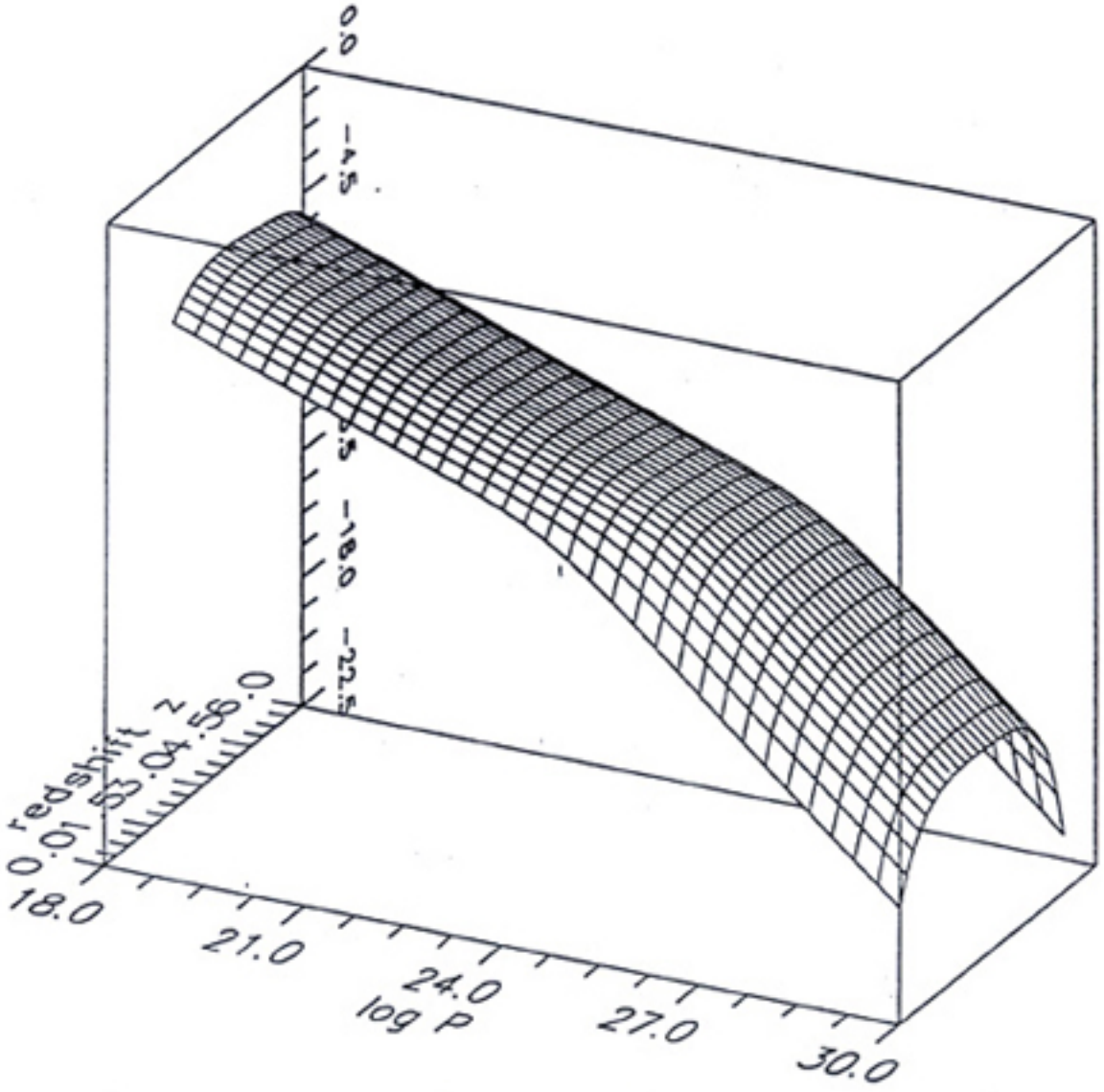

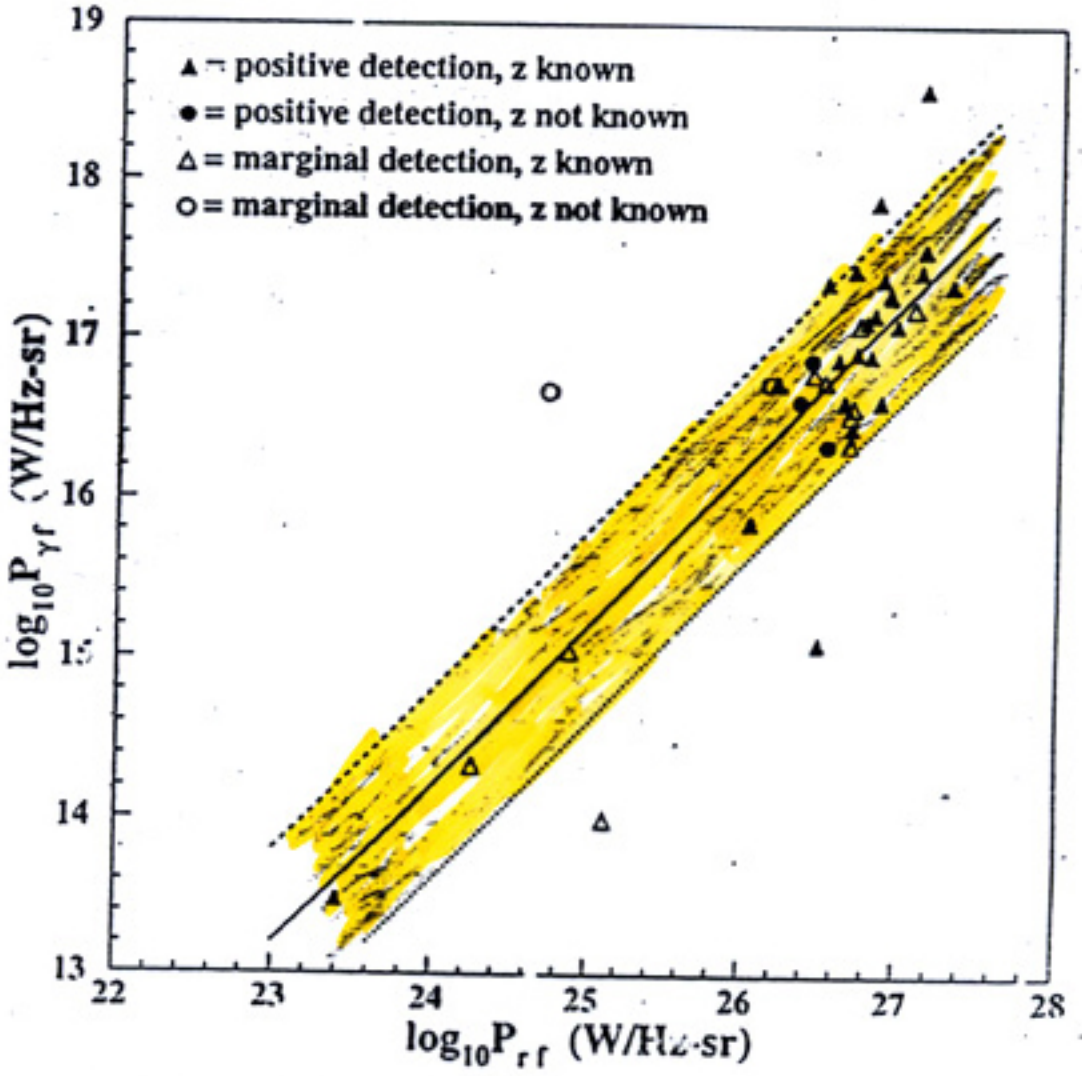

FIG. 2.—Scatter plot of radio (2.7 GHz) and γ-ray (100 MeV) luminosities for the 38 EGRET sources. Sources of unknown redshift are assumed to have $z = 1.00$ for the calculation of the spectral correction factors (eq. [3]), required to obtain absolute luminosities from measured fluxes. The lines represent the relation between the radio and γ-ray luminosities, $P_{\gamma f} = 10^{\xi} P_{rf}$. The solid line corresponds to $\xi = -9.8$, while the dashed and dotted lines respectively correspond to $\xi = -9.2$ and $\xi = -10.4$.

SECOND GENERATION MODEL FOR CALCULATING THE GAMMA-RAY BACKGROUND FROM FAINT UNRESOLVED BLAZARS

- Consider two states, "flaring" and "quiescent".

- Quiescent sources have a slightly steeper spectrum on average than flaring sources.

- Sources spend a fraction of time $\zeta \ll 1$ in the flaring state.

- As a consequence, quiescent sources make up most of the background, whereas the EGRET sample contains a larger fraction of sources in the flaring state, this fraction determined by the high end of the γ-ray luminosity function and the mean flare amplification factor

$$A \equiv \langle \text{ flaring flux } \rangle / \langle \text{ quiescent flux} \rangle$$

$$\rho_\gamma(P_{\gamma f}, z) = (1-\zeta)\eta\rho_r\left(\frac{P_{\gamma f}}{\kappa}, z\right) + \zeta\eta\rho_r\left(\frac{P_{\gamma f}}{A\kappa}, z\right),$$

where the quiescent and flare γ-ray luminosities, P_γ^q and P_γ^f, are related to the radio luminosity as $P_\gamma^q = \kappa P_r$ and $P_\gamma^f = A\kappa P_r$.

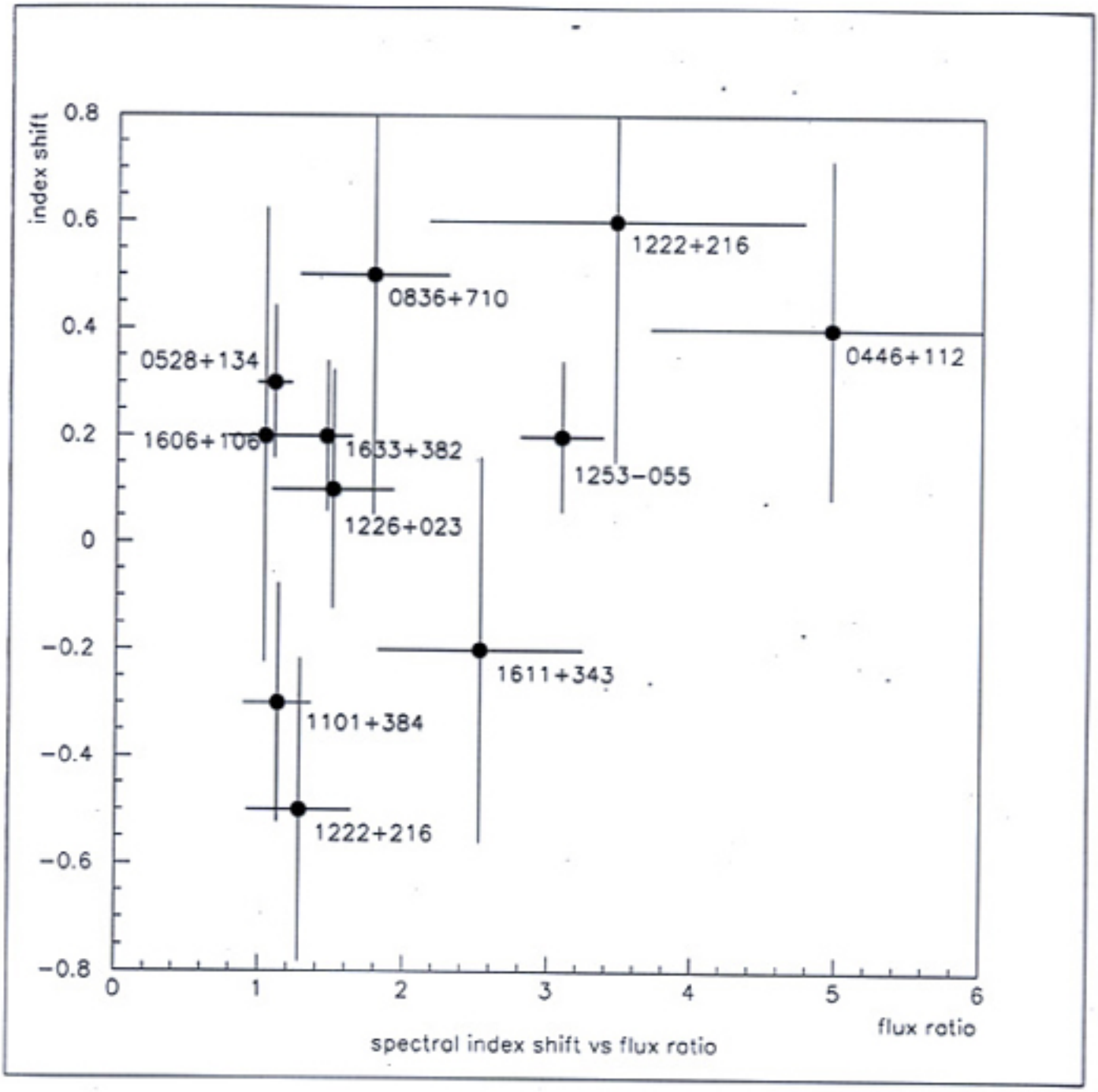

spectral index shift vs flux ratio

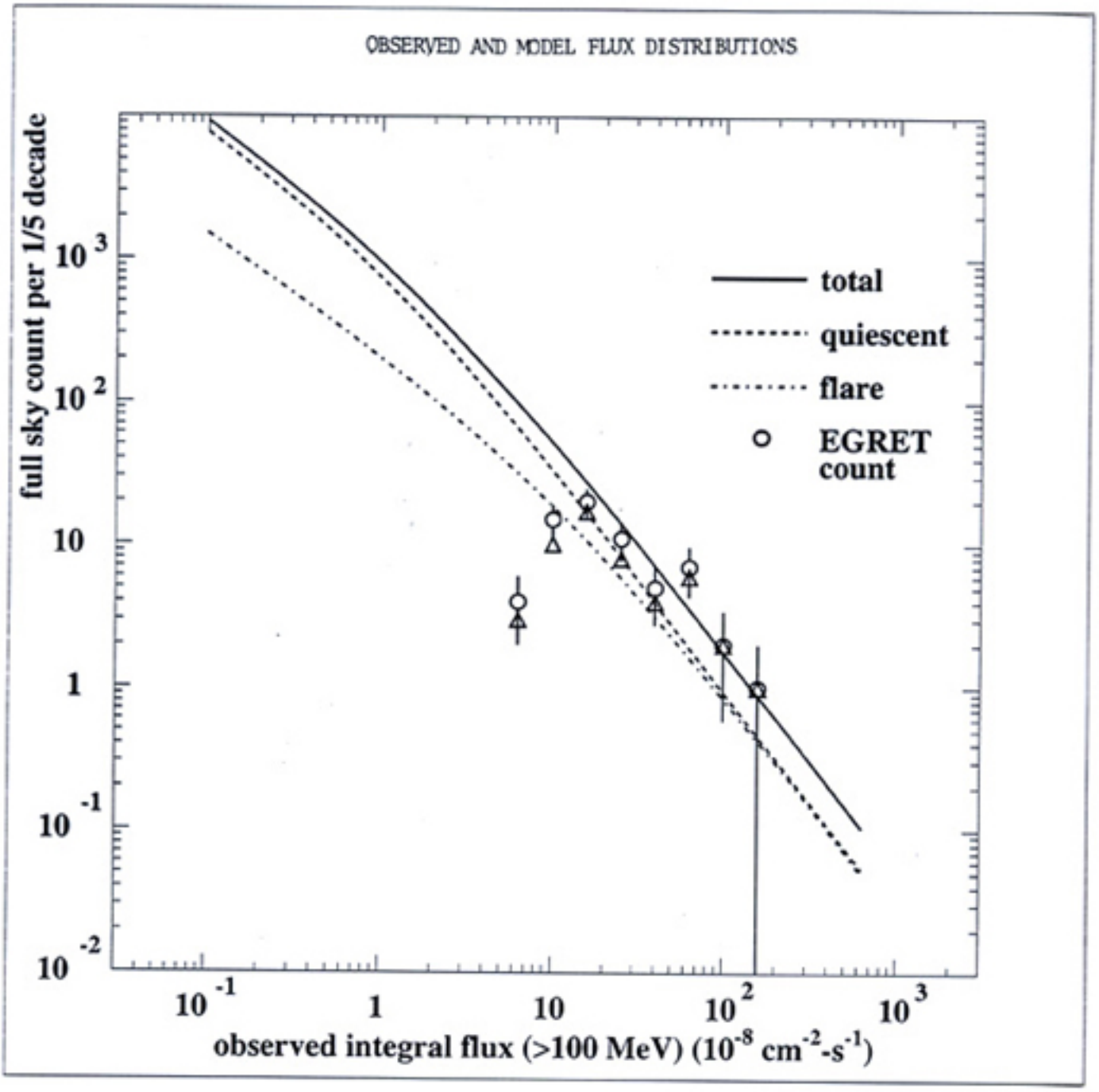

CIRCLES; 50 IDENTIFIED + 14 UNIDENTIFIED SOURCES

TRIANGLES: 50 IDENTIFIED SOURCES (2nd EGRET CATALOGUE)

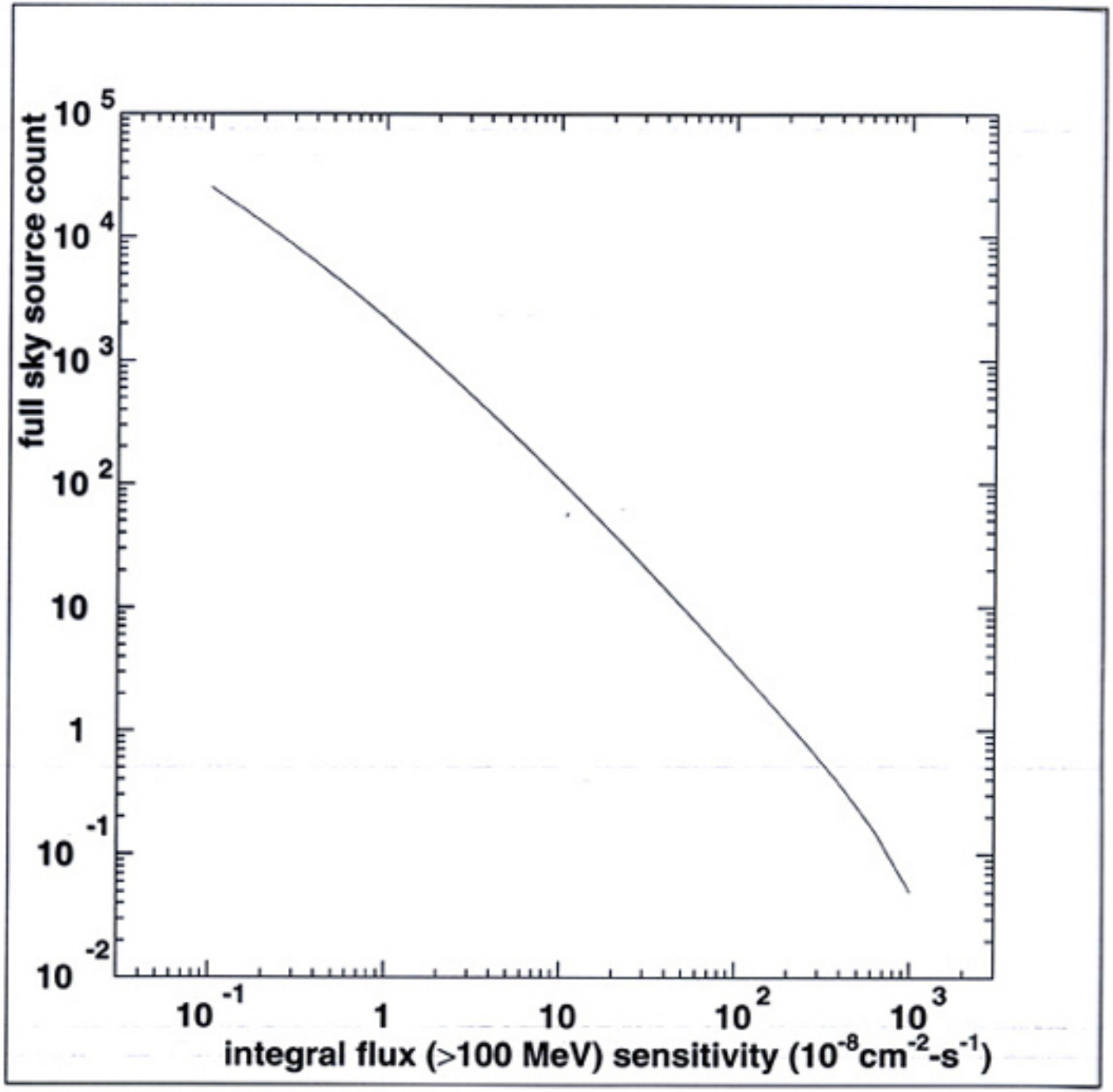
full sky source count
10^{5}
10^{4}
10^{3}
10^{2}
10
1
10^{-1}
10^{-2}
10^{-1}
1
10
10^{2}
10^{3}
integral flux (>100 MeV) sensitivity (10^{-8}cm^{-2}-s^{-1})

One Year Point Source Catalog (2006-2007 ?)

5 σ sources from
Simulated All Sky Survey

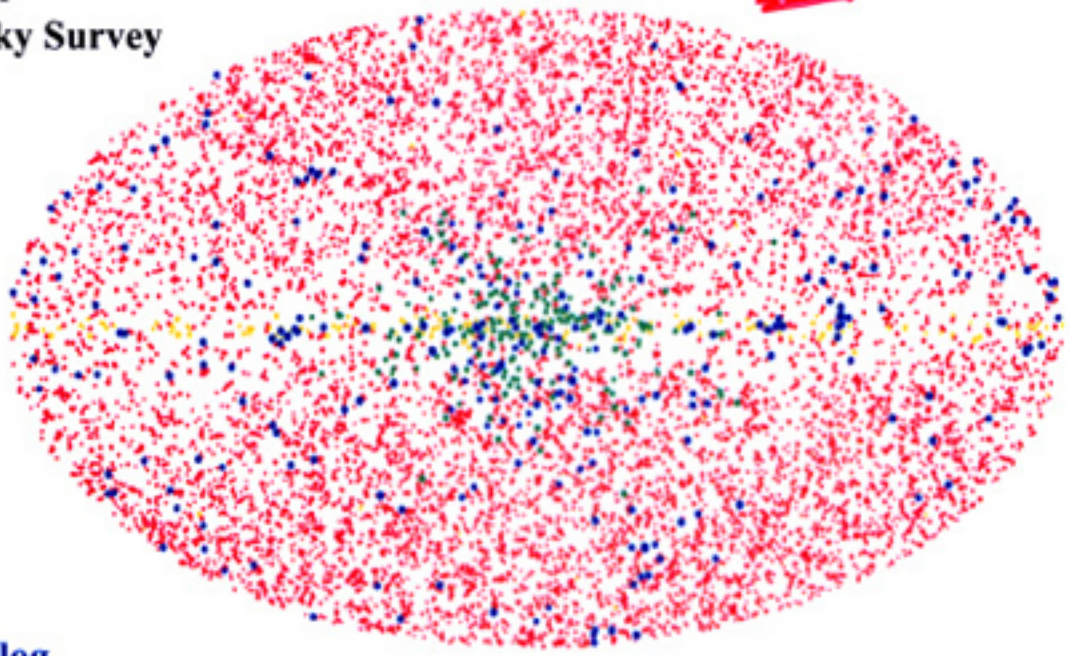

$$\frac{dF}{dE}(E_0) = \frac{c}{H_0 E_f \ln 10}\left\{\int p^q(\alpha)\left(\frac{E_0}{E_f}\right)^{(\alpha+1)}\int_0^{z_{max}}\frac{dz}{(1+z)^{\alpha+5/2}}\int_{P_{r,min}}^{P_{r,max}^q(z)}(1-\zeta)\eta\rho(P_r, z)dP_r\right\}$$
$$+\left\{\int p^f(\alpha)\left(\frac{E_0}{E_f}\right)^{(\alpha+1)}\int_0^{z_{max}}\frac{dz}{(1+z)^{\alpha+5/2}}\int_{P_{r,min}}^{P_{r,max}^f(z)}\zeta\eta\rho(P_r, z)dP_r\right\}.$$

The radio luminosity limits are given by $P^q_{r,max}(z) = P_{rf,max}(z)/\kappa$ and $P^f_{r,max}(z) = P_{rf,max}(z)/A\kappa$.

This equation gives the results shown in Figure 3, plotted as $E^2(dF/dE)$ (the "energy flux") versus E, for the parameter values $\kappa = 4 \times 10^{-11}$, $\eta = 1.0$, $\zeta = 0.03$, $A = 5$, $\Delta\alpha_q = 0.20$, and $\Delta\alpha_f = -0.05$. Both the amplitude and shape of the calculated energy flux $E^2(dF/dE)$ matches that of the data, with the exception of the two end data points, which have large systematic uncertainties (not shown) (P. Sreekumar 1995, personal communication). We note in particular the role of the spectral index shift between the quiescent and flare state populations.

BACKGROUND SPECTRA

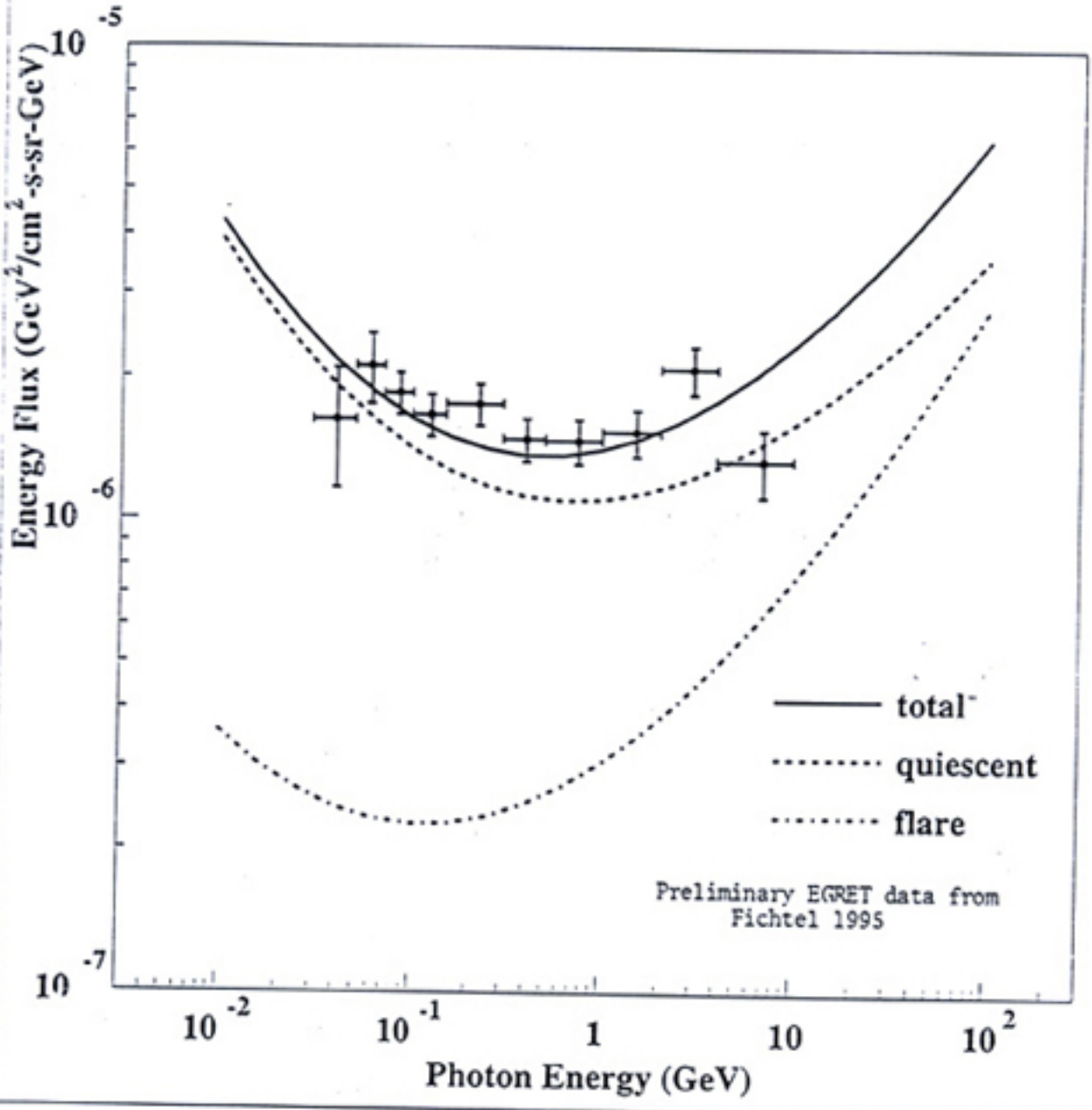

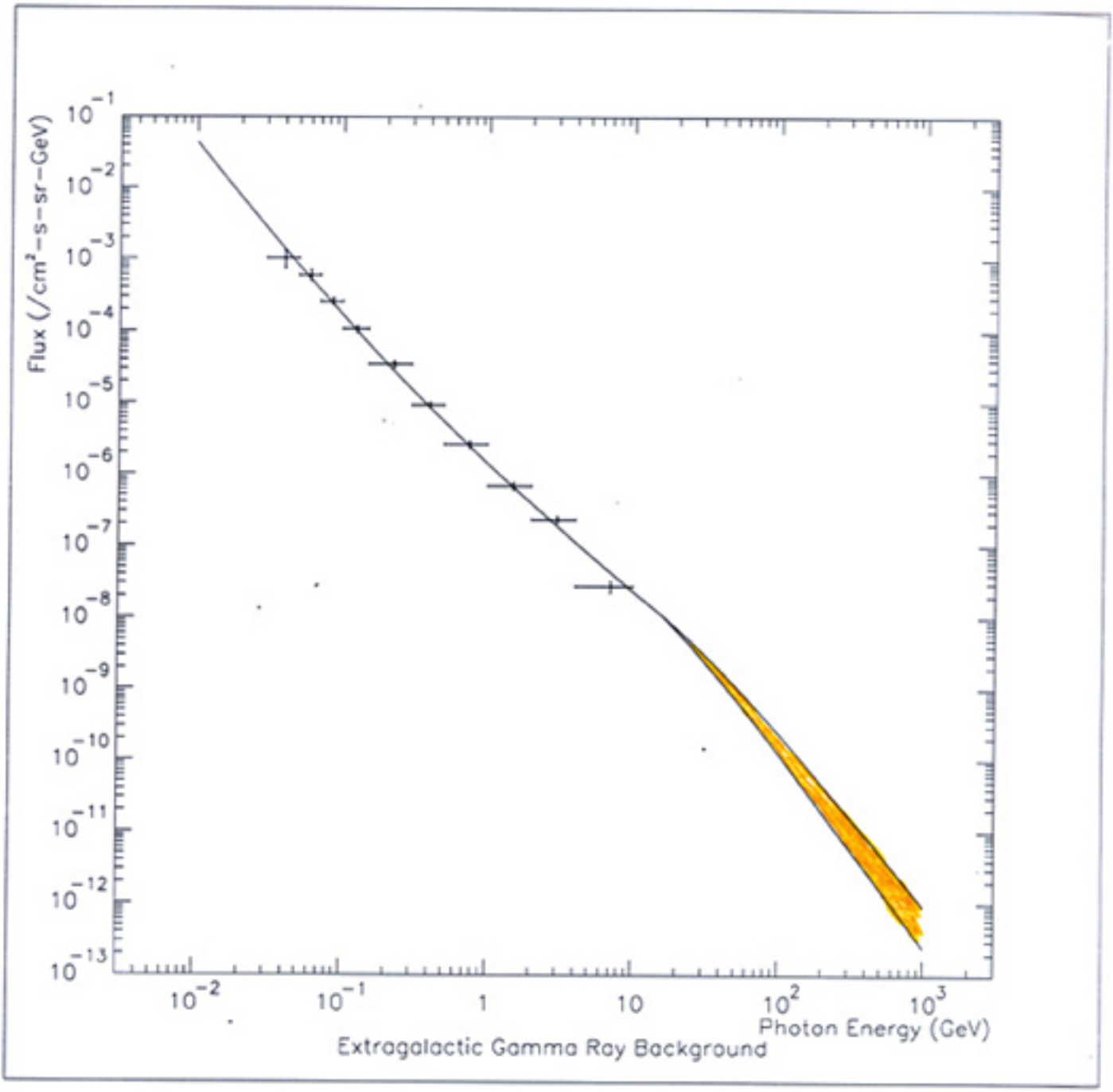

Salamon + Stecker 1996

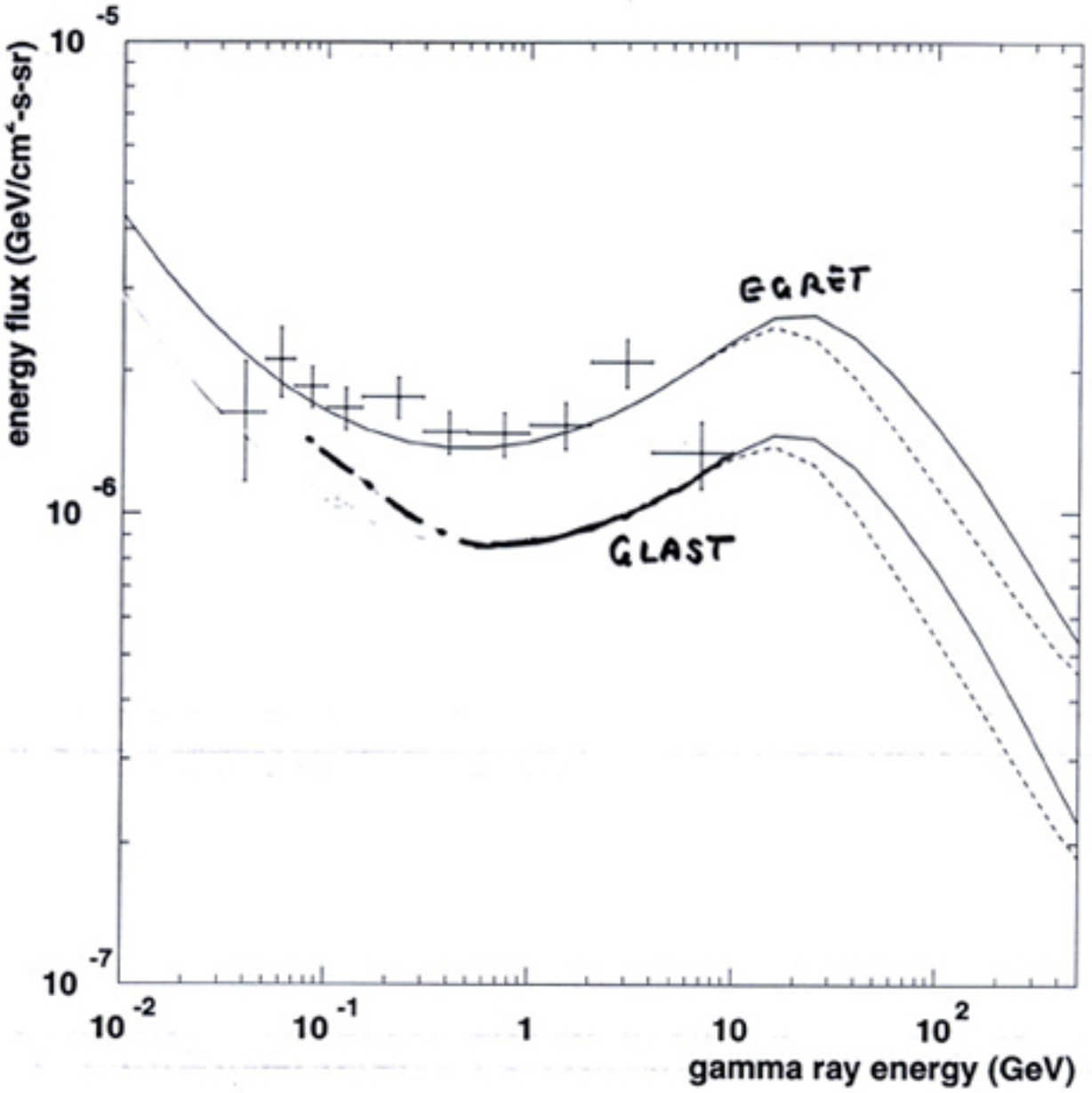

ABOVE ~1 GeV GLAST BG ~ ½ EGRET BG

Conclusions from Stecker & Salamon 1996

- Blazars can account for the dominant part of the EGB observed by EGRET.
- The predicted EGB is slightly concave on a log-log plot below in the GeV range and will steepen above ~20 GeV owing to intergalactic absorption. (Intrinsic blazar spectra may also fall off in this energy range: look for DM lines and other components at ~100 GeV.)
- Quiescent sources should make up most of the background whereas the EGRET sample contains a larger fraction of sources in the flaring state.
- GLAST should resolve about half of the EGRET EGB above 1 GeV and should see ~2000 blazars.

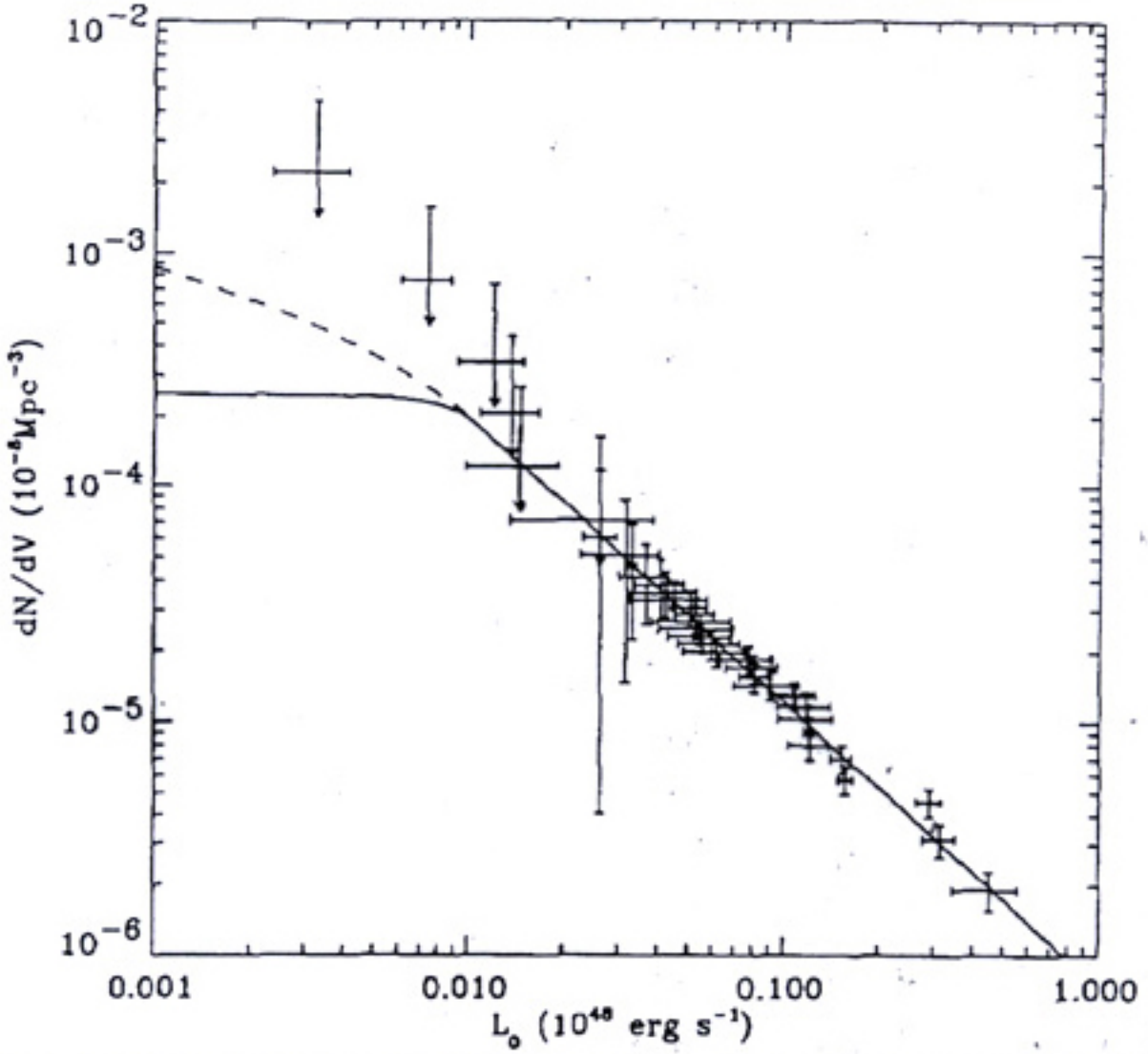

Fig. 1. Cumulative luminosity function derived from the de-evolved luminosities. The data points are the luminosity function estimates using the smoothed nonparametric method of Caditz and Petrosian (1993). The solid line is the cumulative luminosity function derived from a broken power-law differential distribution (Chiang and Mukherjee 1998).

Chiang & Mukherjee Model

- Used Kuehr catalogue to cross correlate.
- LF with *no* sources below 10^{46} erg/s.
- Concluded that only ¼ of background is from unresolved blazars.
- *All 6 EGRET sources with $z < 0.2$ had luminosities between 10^{45} and 10^{46} erg/s!*
- *If there is no radio:γ-ray luminosity correlation, since Kuehr has only 10^{-6} of sources, virtually none of the ~70 EGRET sources would be in the catalogue.*
- Stecker-Salamon: unresolved blazars dominant.

EGB Component from Clusters

- Loeb & Waxman 2000: background is from shock acceleration in forming galaxy clusters.
- Berrington & Dermer 2002: only a small fraction of background from clusters; wrong spectrum predicted.
- Scharf & Mukherjee 2002: 3σ statistical evidence of correlation with clusters (?),

  1-10% of EGB from clusters?

Blazars, the EGB and Absorption: Relevant GLAST Observations

- Need good spectra for hundreds of blazars up to 100 GeV in order to understand γ–ray production mechanisms and the EGB.
- Need demographic profile of blazar types, *i.e.*, number *vs.* peak SED energy in order to understand the EGB.
- Need to determine the source count curve (number *vs.* flux) and luminosity function for hundreds of blazars.